J|A|C|S
ARTICLES
Published on Web 05/15/2002

Mechanism of Asymmetric Hydrogenation of α-(Acylamino)acrylic Esters Catalyzed by BINAP−Ruthenium(II) Diacetate

Masato Kitamura,* Masaki Tsukamoto, Yuhki Bessho, Masahiro Yoshimura, Uwe Kobs, Michael Widhalm, and Ryoji Noyori*

Contribution from the Department of Chemistry and Research Center for Materials Science, Nagoya University, Chikusa, Nagoya 464-8602, Japan

Received April 17, 2001

Abstract: The mechanism of asymmetric hydrogenation of α-(acylamino)acrylic esters with $Ru(CH_3COO)_2$-[(*S*)-binap] (BINAP = 2,2′-bis(diphenylphosphino)-1,1′-binaphthyl), giving the *S* saturated products in >90% ee, has been investigated by means of a kinetic study, deuterium labeling experiments, isotope effect measurements, and NMR and X-ray analysis of certain Ru complexes. The hydrogenation in methanol under a low H_2 pressure proceeds via a monohydride-unsaturate mechanism that involves the initial RuH formation followed by a reaction with an olefinic substrate. The migratory insertion in the enamide−RuH chelate complex occurs reversibly and endergonically in an exo manner, giving a five-membered metallacycle intermediate. The cleavage of the Ru−C bond is achieved with either H_2 (major) or CH_3OH (minor). Both of the pathways result in overall cis hydrogenation products. The hydrogen at C(3) is mainly from an H_2 molecule, and the C(2) hydrogen is from another H_2 or protic CH_3OH. The major *S* and minor *R* enantiomers are produced via the same mechanism involving diastereomeric intermediates. The turnover rate is limited by the step of hydrogenolysis of a half-hydrogenated metallacyclic intermediate. The participation of two different hydrogen donor molecules is in contrast to the pairwise dihydrogenation using a single H_2 molecule in the Rh(I)-catalyzed reaction which occurs via a dihydride mechanism. In addition, the sense of asymmetric induction is opposite to that observed with (*S*)-BINAP−Rh(I) catalysts. The origin of this phenomenon is interpreted in terms of stereocomplementary models of the enamide/metal chelate complexes. A series of model stoichiometric reactions mimicking the catalytic steps has indicated that most NMR-observable Ru complexes are not directly involved in the catalytic hydrogenation but are reservoirs of real catalytic complexes or even side products that retard the reaction.

Introduction

Asymmetric hydrogenation of olefins catalyzed by chiral phosphine-transition metal complexes has created a tremendous potential in organic synthesis.[1] In particular, the Rh-catalyzed enantioselective hydrogenation of N-acylated dehydroamino acids or their esters now constitutes a standard tool for the synthesis of natural and unnatural amino acids of high enantiomeric purity.[2,3] Halpern and Brown, among others, studied extensively the pathways of asymmetric hydrogenation of methyl (*Z*)-α-(acetamido)cinnamate [(*Z*)-**1**] and related compounds in alcohol containing a cationic DIPAMP− or CHIRAPHOS−Rh complex,[4−6] and they concluded that the unsaturate-dihydride mechanism operates as illustrated in Figure 1. The cationic diphosphine−Rh(I) complex **5** first interacts with a bidentate enamide substrate to give the chelate complex **6**, to which molecular hydrogen undergoes oxidative addition. The resulting Rh(III) dihydride **7** causes the successive transfer of the two hydrogen atoms to the coordinated olefinic bond. The

* To whom correspondence should be addressed. E-mail: noyori@chem3.chem.nagoya-u.ac.jp.

(1) Reviews: (a) Noyori, R. *Asymmetric Catalysis in Organic Synthesis*; John Wiley: New York, 1994. (b) Takaya, H.; Ohta, T.; Noyori, R. In *Catalytic Asymmetric Synthesis*; Ojima, I., Ed.; VCH: Weinheim, 1993; Chapter 1. (c) *Chirality in Industry*; Collins, A. N., Sheldrake, G. N., Crosby, J., Eds.; Wiley: New York, 1992. (d) Noyori, R. *CHEMTECH* **1992**, 360−367. (e) Noyori, R. *Science* **1990**, *248*, 1194−1199. (f) Noyori, R.; Takaya, H. *Acc. Chem. Res.* **1990**, *23*, 345−350. (g) Noyori, R.; Kitamura, M. In *Modern Synthetic Methods*; Scheffold, R., Ed.; Springer-Verlag: Berlin, 1989; pp 115−198. (h) Noyori, R. *Chem. Soc. Rev.* **1989**, *18*, 187−208. (i) Nógrádi, M. *Stereoselective Synthesis*; VCH: Weinheim, 1987. (j) Bosnich, B. *Asymmetric Catalysis*; Martinus Nijhoff: Dordrecht, 1986. (k) *Asymmetric Synthesis*; Morrison, J. D., Ed.; Academic Press: New York, 1985; Vol. 5.

(2) The first report: (a) Dang, T. P.; Kagan, H. B. *J. Chem. Soc., Chem. Commun.* **1971**, 481. *N*-Acetyl phenylalanine in >80% enantiomeric excess (ee) was obtained by use of a DIOP-Rh(I) complex (DIOP = 2,3-*O*-isopropylidene-2,3-dihydroxy-1,4-bis(diphenylphosphino)butane). For recent advancements in the chiral Rh complex-catalyzed asymmetric hydrogenation, see: (b) Brown, J. M. In *Comprehensive Asymmetric Catalysis*; Jacobsen, E., Pfaltz, A., Yamamoto, H., Eds.; Springer-Verlag: Berlin, 1999; Vol. I, Chapter 5.1. (c) Ohkuma, T.; Kitamura, M.; Noyori, R. In *Catalytic Asymmetric Synthesis*, 2nd ed.; Ojima, I., Ed.; VCH: Weinheim, 2000; Chapter 1.3. (d) Burk, M. J.; Bienewald, F. In *Transition Metals for Organic Chemistry*; Beller, M., Bolm, C., Eds.; Wiley-VCH: Weinheim, 1998; Vol. 2, Chapter 1.3.

(3) Miyashita, A.; Yasuda, A.; Takaya, H.; Toriumi, K.; Ito, T.; Souchi, T.; Noyori, R. *J. Am. Chem. Soc.* **1980**, *102*, 7932−7934.

(4) (a) Chan, A. S. C.; Pluth, J. J.; Halpern, J. *J. Am. Chem. Soc.* **1980**, *102*, 5952−5954. (b) Halpern, J. *Inorg. Chim. Acta* **1981**, *50*, 11−19. (c) Halpern, J. *Acc. Chem. Res.* **1982**, *15*, 332−338. (d) Halpern, J. *Pure Appl. Chem.* **1983**, *55*, 99−106. (e) Landis, C. R.; Halpern, J. *J. Am. Chem. Soc.* **1987**, *109*, 1746−1754. (f) McCulloch, B.; Halpern, J.; Thompson, M. R.; Landis, C. R. *Organometallics* **1990**, *9*, 1392−1395. (g) Halpern, J. *Precious Met.* **1995**, *19*, 411−421.

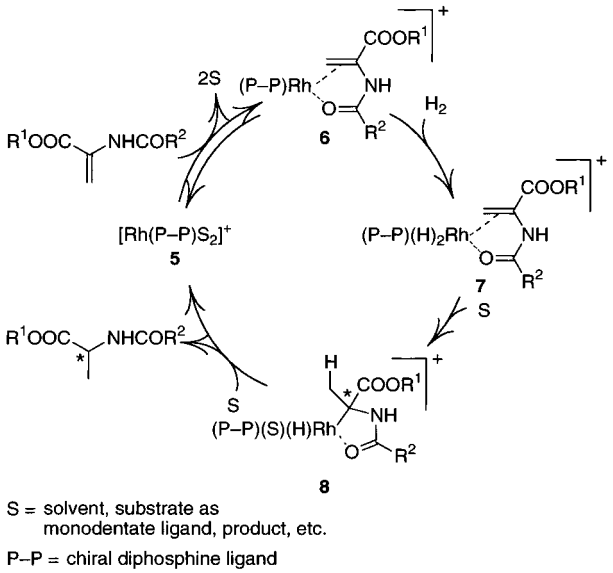

Figure 1. Catalytic cycle of the Rh(I)-catalyzed hydrogenation of N-acylated dehydroamino esters. β-Substituents are omitted for clarity.

olefin migratory insertion in the dihydride **7** followed by the reductive elimination of the five-membered organorhodium hydride **8** gives the saturated product and **5**. The overall cis hydrogenation using a single H_2 molecule is achieved by the cis olefin insertion in **7** and the hydride transfer in **8** with retention of the configuration.[7] When a C_2 chiral diphosphine is used, the enamide complex **6** could be a mixture of diastereomers, depending on the enantioface selection. The overall enantioselectivity is determined by multiplication of the equilibrium concentrations of the stereoisomers and their relative reactivities. Remarkably, the less stable, minor isomer of **6** has proved more reactive toward H_2, overwhelming the relative stabilities, to afford the major enantiomer.[8,9] A recent detailed theoretical study suggests the possibility that the oxidative addition of H_2 to **6** is endergonic and reversible and that the olefin/Rh−H migratory insertion, **7** → **8**, constitutes the turnover-limiting step.[10] In addition to this standard pathway, alternative dihydride-unsaturate mechanisms have also been postulated.[11,12] The formation of a RhH_2 may precede the olefin−Rh interaction, depending on the chiral ligands and reaction conditions.

Reactions using Ru(II) complexes, particularly with a BINAP ligand,[3,13] find a wider synthetic scope, allowing asymmetric hydrogenation of a range of functionalized olefins including enamides,[14,15] α,β- and β,γ-unsaturated carboxylic acids,[16] and allylic and homoallylic alcohols,[17] as well as various functionalized ketones.[18,19] The mechanism of the Ru-catalyzed hydrogenation, however, is multifarious, and only limited cases have been fully clarified.[20−24] Most interestingly, the Rh and Ru complexes with the same chiral diphosphine often exhibit an opposite sense of asymmetric induction in the hydrogenation of (*Z*)-α-(acylamino)acrylic acids or esters.[3,25] As illustrated in Figure 2, in the presence of (*S*)-**9**, a cationic (*S*)-BINAP−Rh complex, (*Z*)-α-(benzamido)cinnamic acid or the methyl ester is hydrogenated in ethanol to give the *R* hydrogenation product in 93−100% ee,[3] whereas the acetamido ester (*Z*)-**1** in methanol gives the *R* product in 61% ee. In contrast, (*S*)-BINAP−Ru complexes afford the *S* enantiomers in up to 92% ee.[15,26] For example, (*S*)-**10** hydrogenates (*Z*)-**1** or the simple, nonphenylated substrate **3** to give the *S* products equally in 90% ee.

(5) (a) Brown, J. M.; Chaloner, P. A. *Tetrahedron Lett*. **1978**, *19*, 1877−1880. (b) Brown, J. M.; Chaloner, P. A. *J. Chem. Soc., Chem. Commun.* **1978**, 321−322. (c) Brown, J. M.; Chaloner, P. A. *J. Chem. Soc., Chem. Commun.* **1980**, 344−346. (d) Brown, J. M.; Murrer, B. A. *Tetrahedron Lett*. **1980**, *21*, 581−584. (e) Brown, J. M.; Chaloner, P. A. *J. Am. Chem. Soc*. **1980**, *102*, 3040−3048. (f) Brown, J. M.; Murrer, B. A. *J. Chem. Soc., Perkin Trans. 2* **1982**, 489−497. (g) Brown, J. M.; Parker, D. *Organometallics* **1982**, *1*, 950−956. (h) Brown, J. M.; Chaloner, P. A.; Morris, G. A. *J. Chem. Soc., Chem. Commun*. **1983**, 664−666. (i) Brown, J. M.; Maddox, P. J. *J. Chem. Soc., Chem. Commun.* **1987**, 1276−1278. (j) Brown, J. M.; Guiry, P. J.; Wienand, A. In *Principle of Molecular Recognition*; Buckingham, A. D., Legon, A. C., Roberts, S. M., Eds.; Blackie: Glasgow, 1993; pp 79−107.

(6) DIPAMP = 1,2-bis[(*o*-methoxyphenyl)phenylphosphino)]ethane. CHIRAPHOS = 2,3-bis(diphenylphosphino)butane.

(7) For the participation of protic solvents at the Rh hydride stage, see: Bakos, J.; Karaivanov, R.; Laghmari, M.; Sinou, D. *Organometallics* **1994**, *13*, 2951−2956.

(8) Many chiral diphosphine ligands that form a λ configurated Rh complex yield (*S*)-α-amino acids, whereas phosphines that form the δ structure yield the *R* enantiomers as major products. See: (a) Fryzuk, M. D.; Bosnich, B. *J. Am. Chem. Soc*. **1977**, *99*, 6262−6267. (b) Fryzuk, M. D.; Bosnich, B. *J. Am. Chem. Soc*. **1978**, *100*, 5491−5494. (c) Vineyard, B. D.; Knowles, W. S.; Sabacky, M. J.; Bachman, G. L.; Weinkauff, D. J. *J. Am. Chem. Soc*. **1977**, *99*, 5946−5952.

(9) For possible discrepancies inferred from the geometries of chiral diphosphines, see: (a) Burk, M. J.; Feaster, J. E.; Nugent, W. A.; Harlow, R. L. *J. Am. Chem. Soc*. **1993**, *115*, 10125−10138. (b) Robin, F.; Mercier, F.; Ricard, L.; Mathey, F.; Spagnol, M. *Chem.-Eur. J*. **1997**, *3*, 1365−1369. (c) Marinetti, A.; Kruger, V.; Buzin, F.-X. *Tetrahedron Lett*. **1997**, *38*, 2947−2950. (d) Imamoto, T.; Watanabe, J.; Wada, Y.; Masuda, H.; Yamada, H.; Tsuruta, H.; Matsukawa, S.; Yamaguchi, K. *J. Am. Chem. Soc*. **1998**, *120*, 1635−1636. (e) Yamanoi, Y.; Imamoto, T. *J. Org. Chem*. **1999**, *64*, 2988−2989. (f) Marinetti, A.; Jus, S.; Genêt, J.-P. *Tetrahedron Lett*. **1999**, *40*, 8365−8368.

(10) Landis, C. R.; Hilfenhaus, P.; Feldgus, S. *J. Am. Chem. Soc.* **1999**, *121*, 8741−8754.

(11) (a) Ojima, I.; Kogure, T.; Yoda, N. *J. Org. Chem*. **1980**, *45*, 4728−4739. (b) Sinou, D. *Tetrahedron Lett*. **1981**, *22*, 2987−2990. (c) Harthun, A.; Kadyrov, R.; Selke, R.; Bargon, J. *Angew. Chem., Int. Ed. Engl*. **1997**, *36*, 1103−1105. (d) Kuwano, R.; Ito, Y. *J. Org. Chem*. **1999**, *64*, 1232−1237.

(12) (a) Gridnev, I. D.; Yamanoi, Y.; Higashi, N.; Tsuruta, H.; Yasutake, M.; Imamoto, T. *Adv. Synth. Catal*. **2001**, *343*, 118−136. (b) Gridnev, I. D.; Higashi, N.; Asakura, K.; Imamoto, T. *J. Am. Chem. Soc*. **2000**, *122*, 7183−7194.

(13) BINAP = 2,2′-bis(diphenylphosphino)-1,1′-binaphthyl.

(14) (a) Noyori, R.; Ohta, M.; Hsiao, Yi; Kitamura, M.; Ohta, T.; Takaya, H. *J. Am. Chem. Soc.* **1986**, *108*, 7117−7119. (b) Kitamura, M.; Hsiao, Yi; Noyori, R.; Takaya, H. *Tetrahedron Lett.* **1987**, *28*, 4829−4832. (c) Kitamura, M.; Hsiao, Yi; Ohta, M.; Tsukamoto, M.; Ohta, T.; Takaya, H.; Noyori, R. *J. Org. Chem.* **1994**, *59*, 297−310.

(15) Kitamura, M.; Yoshimura, M.; Tsukamoto, M.; Noyori, R. *Enantiomer* **1996**, *1*, 281−303.

(16) Ohta, T.; Takaya, H.; Kitamura, M.; Nagai, K.; Noyori, R. *J. Org. Chem*. **1987**, *52*, 3174−3176.

(17) Takaya, H.; Ohta, T.; Sayo, N.; Kumobayashi, H.; Akutagawa, S.; Inoue, S.; Kasahara, I.; Noyori, R. *J. Am. Chem. Soc.* **1987**, *109*, 1596−1597, 4129.

(18) (a) Noyori, R.; Ohkuma, T.; Kitamura, M.; Takaya, H.; Sayo, N.; Kumobayashi, H.; Akutagawa, S. *J. Am. Chem. Soc.* **1987**, *109*, 5856−5858. (b) Kitamura, M.; Ohkuma, T.; Inoue, S.; Sayo, N.; Kumobayashi, H.; Akutagawa, S.; Ohta, T.; Takaya, H.; Noyori, R. *J. Am. Chem. Soc*. **1988**, *110*, 629−631. For reviews, see: (c) Ohkuma, T.; Kitamura, M.; Noyori, R. In *Catalytic Asymmetric Synthesis*, 2nd ed.; Ojima, I., Ed.; VCH: Weinheim, 2000; Chapter 1.4.1. (d) Genêt, J. P. In *Reductions in Organic Synthesis: Recent Advances and Practical Applications (ACS. symposium series 641)*; Abdel-Magid, A. F., Ed.; American Chemical Society: Washington, DC, 1996; Chapter 2.

(19) For asymmetric hydrogenation of simple, unfunctionalized ketones, see: Noyori, R.; Ohkuma, T. *Angew. Chem., Int. Ed*. **2001**, *40*, 40−73.

(20) Ashby, M. T.; Halpern, J. *J. Am. Chem. Soc.* **1991**, *113*, 589−594.

(21) Ohta, T.; Takaya, H.; Noyori, R. *Tetrahedron Lett.* **1990**, *31*, 7189−7192.

(22) Wiles, J. A.; Bergens, S. H.; Young, V. G. *J. Am. Chem. Soc.* **1997**, *119*, 2940−2941.

(23) Wiles, J. A.; Bergens, S. H. *Organometallics* **1998**, *17*, 2228−2240.

(24) Wiles, J. A.; Bergens, S. H. *Organometallics* **1999**, *18*, 3709−3714.

(25) (a) Miyashita, A.; Takaya, H.; Souchi, T.; Noyori, R. *Tetrahedron* **1984**, *40*, 1245−1253. (b) Kawano, H.; Ikariya, T.; Ishii, Y.; Saburi, M.; Yoshikawa, S.; Uchida, Y.; Kumobayashi, H. *J. Chem. Soc., Perkin Trans. 1* **1989**, 1571−1575. (c) Noyori, R.; Ikeda, T.; Ohkuma, T.; Widhalm, M.; Kitamura, M.; Takaya, H.; Akutagawa, S.; Sayo, N.; Saito, T.; Taketomi, T.; Kumobayashi, H. *J. Am. Chem. Soc.* **1989**, *111*, 9134−9135. (d) Lubell, W. D.; Kitamura, M.; Noyori, R. *Tetrahedron: Asymmetry* **1991**, *2*, 543−554.

(26) Ikariya, T.; Ishii, Y.; Kawano, H.; Arai, T.; Saburi, M.; Yoshikawa, S.; Akutagawa, S. *J. Chem. Soc., Chem. Commun*. **1985**, 922−924.

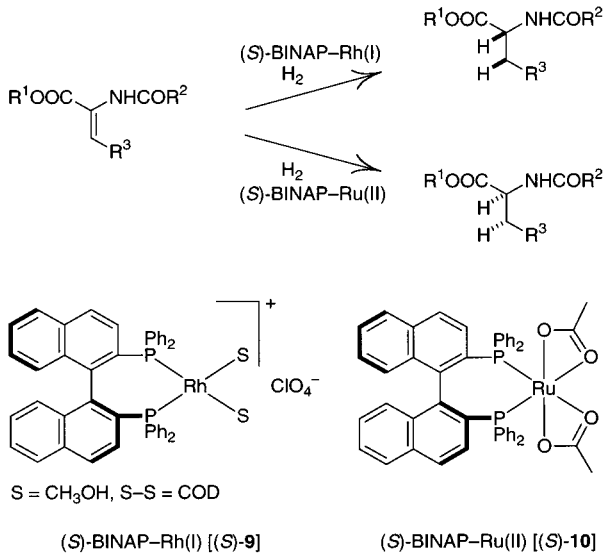

Figure 2. Asymmetric hydrogenation of α-(acylamino)acrylic esters by (*S*)-BINAP−Rh(I) or −Ru(II) complexes.

We have studied the mechanism and the origin of unique enantioselection in the Ru(II)-catalyzed hydrogenation of enamides by means of kinetic measurement, deuterium labeling experiments, determining isotope effects, and ^{1}H and ^{31}P NMR and X-ray analysis of some BINAP−Ru complexes. The investigation, performed with (*S*)-**10**, a neutral Ru(II) complex, in methanol, has led to the conclusion that, in contrast to the Rh-catalyzed reaction involving a Rh dihydride intermediate, this hydrogenation proceeds via a Ru monohydride species as we proposed earlier.[15] Recent work by Bergens et al. using (*Z*)-**1**, [RuH[(*R*)-binap](CH$_3$CN)$_n$S$_{3-n}$]BF$_4$ (n = 0−3, S = acetone or methanol) as a preformed cationic Ru(II)H catalyst,[22−24] and acetone or THF as a solvent, disclosed many intriguing mechanistic aspects which are different from those in the Rh-catalyzed hydrogenation. In homogeneous hydrogenation of olefins, neutral and cationic transition metal complexes often behave differently in a qualitative[4,27] or quantitative sense.[27] In addition, the acetate ligand which serves as either a 2e donor or a hemilabile 4e donor may play a special role in stabilizing and activating the catalytic species. Protic methanol would facilitate the monodentate/bidentate exchange process. Thus, this and Bergens' investigations complementarily pave the way for a deep understanding of the mechanism of Ru-catalyzed asymmetric hydrogenation of enamides.

Results and Discussion

Standard Reactions. Methyl (*Z*)-α-(acetamido)cinnamate [(*Z*)-**1**] was selected as a standard probe substrate. The simple acrylic analogue **3** was also used for some purposes. The hydrogenation was first performed in methanol under the conditions of [(*S*)-**10**]$_0$ = 0.75 mM, [(*Z*)-**1**]$_0$ = 150 mM, 1 atm H$_2$, and 30 °C. The reaction gave (*S*)-**2** in 90% ee in 78% yield after 3−4 h and in 100% yield after 24 h. Hydrogenation at 0 °C was slower by a factor of 100 than the reaction at 30 °C, while the product ee was increased to 96%.[28] Unlike in the Rh-catalyzed reaction,[3] enantioselectivity was insensitive to substrate concentration within a range from 400 to 100 mM and also to catalyst concentration in a range from 2 to 0.1 mM. On the other hand, hydrogen pressure had a profound effect on the enantioselectivity[15,28] and reaction rate. The ee's of 90−92% were obtained in a range from 0.1 to 2 atm, but the value was decreased to 87% at 3 atm, 80% at 10 atm, and even 70% at 100 atm. The reaction was accelerated sharply by an increase of the hydrogen pressure from 0.3 to 1.2 atm, but, at higher pressure, the effect became weak or even negative.[15,29] The reaction at 100 atm in an autoclave was ca. 5 times slower than that at 1 atm, implying that there was a change in the mechanism. The nonphenylated substrate **3** was converted quantitatively to (*S*)-**4** in 90% ee after 4−5 h under the standard conditions. Such findings indicate the operation of dual mechanisms depending on the H$_2$ pressure particularly at higher pressure. Thus, this mechanistic study deals with only hydrogenation at 0.6−1.2 atm as the standard reactions which displayed the constant product ee (90−92%) and a linear increase in rate as a function of H$_2$ pressure. At H$_2$ pressure as low as 0.3 atm, this reaction suffers mass transfer problem which results in the slight deviation from the linearity, because the actual H$_2$ concentration in solution is lower than that estimated from the pressure.[30,31]

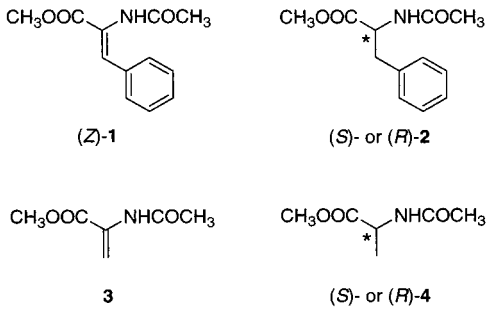

Catalytic Cycle. Many characteristics of the BINAP−Rh(I)-catalyzed reaction are in accord with the unsaturate-dihydride mechanism of Figure 1, in which an initially formed Rh−enamide complex reacts with H$_2$. We here propose that the hydrogenation of enamides catalyzed by the Ru complex (*S*)-**10** under the standard conditions proceeds via the monohydride-unsaturate mechanism outlined in Figure 3. This mechanism is characterized by the formation of a Ru monohydride prior to olefin coordination. First, the precatalyst **10** cleaves molecular hydrogen via an η^2-H$_2$ complex[32,33] in a heterolytic fashion[20,34,35] to give the Ru(II) monohydride **11** and acetic acid. The Ru species **11** interacts with an enamide to form the short-lived complex **12**, in which olefin insertion into the Ru−H bond forms

(27) Collman, J. P.; Hegedus, L. S.; Norton, J. R.; Finke, R. G. *Principles and Application of Organotransition Metal Complexes*; University Science Books: Mill Valley, CA, 1987.
(28) A similar observation was made by Bergens in a study using (*Z*)-**1** as substrate and [RuH[(*R*)-binap](CH$_3$CN)$_n$S$_{3-n}$]BF$_4$ (n = 0−3, S = acetone or methanol) as catalyst.[23,24]
(29) The rate is affected mechanically by reaction conditions including the way and rate of stirring and reaction vessels.
(30) Sun, Y.; Landau, R. N.; Wang, J.; LeBlond, C.; Blackmond, D. G. *J. Am. Chem. Soc.* **1996**, *118*, 1348−1353.
(31) This was confirmed by the experiment at 0.3 atm H$_2$ pressure, where reaction at ca. 900 rpm occurred about 3 times faster than that at 0 rpm in the early stages.
(32) Morris, R. H. *Can. J. Chem.* **1996**, *74*, 1907−1915.
(33) Jessop, P. G.; Morris, R. H. *Coord. Chem. Rev.* **1992**, *92*, 155−284.
(34) (a) Giovannetti, J. S.; Kelly, C. M.; Landis, C. R. *J. Am. Chem. Soc.* **1993**, *115*, 4040−4057. (b) Brown, J. M. *Chem. Soc. Rev.* **1993**, 25−41. (c) Brown, J. M.; Rose, M.; Knight, F. I.; Wienand, A. *Recl. Trav. Chim. Pays-Bas* **1995**, *114*, 242−251. (d) Chan, A. S. C.; Chen, C. C.; Yang, T. K.; Huang, J. H.; Lin, Y. C. *Inorg. Chim. Acta* **1995**, *234*, 95−100.
(35) (a) Brown, J. M.; Evans, P. L. *Tetrahedron* **1988**, *44*, 4905−4916. (b) Bogdan, P. L.; Irwin, J. J.; Bosnich, B. *Organometallics* **1989**, *8*, 1450−1453.

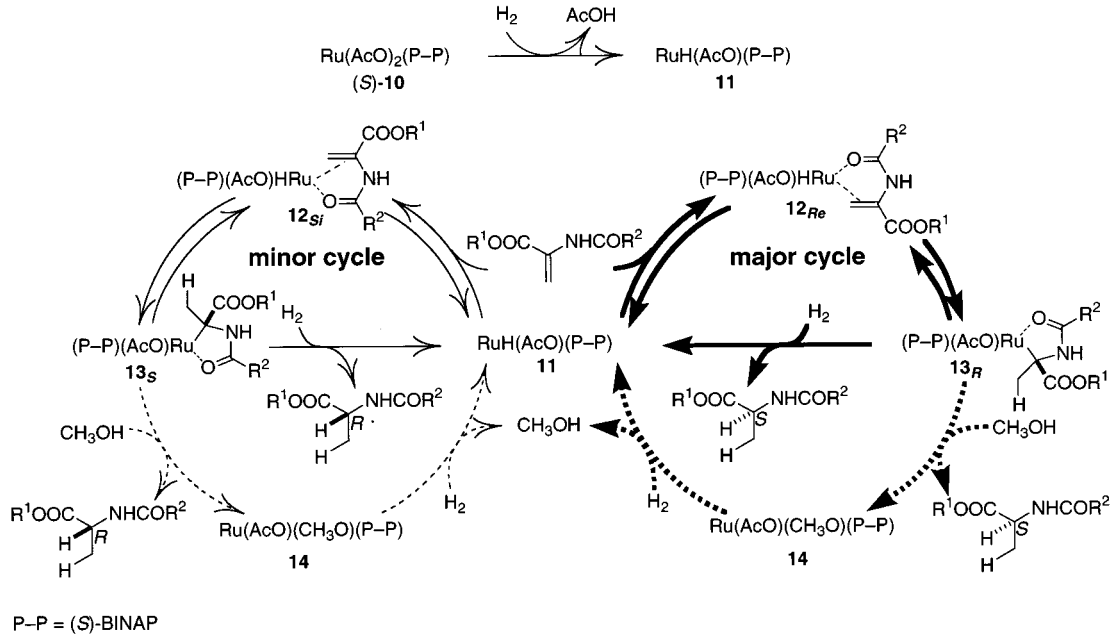

Figure 3. Mechanism of (*S*)-BINAP−Ru-catalyzed hydrogenation of α-(acylamino)acrylic esters in methanol. *β*-Substituents in the substrates are omitted for clarity.

the five-membered metallacycle **13**.[36] This exo cyclization is kinetically and thermodynamically favored over the endo reaction which gives the six-membered compound.[10] The migratory insertion is reversible. The Ru−C bond in **13** is then cleaved by H_2 to afford the catalytic monohydride **11** with release of the saturated product, completing the catalytic cycle. In addition, the Ru−C linkage in **13** is cleaved partly by a coordinated methanol molecule to form the product and the Ru(II) species **14**. In this case, hydrogenolysis of the Ru−OCH_3 bond in **14**[20,21] revives the catalyst **11**. Alternatively, **14** might undergo prior protonation to the CH_3O ligand or CH_3O/AcO ligand exchange, giving **10**, and then react with H_2. This mechanistic scheme shows a kinetically formed Ru species, many of which are apparently coordinatively unsaturated. Although many 14e and 16e Ru(II) complexes are known,[37,38] the catalytic complexes could in fact be stabilized by internal coordination of the acetate ligand as a hemilabile 4e donor or the BINAP ligand as the 6e donor,[39] or by the ligation of methanol, substrate, or product molecule(s). The stereochemistry of the product is determined in the Ru−C cleavage steps, **13** → **11** and **13** → **14**, which occur irreversibly with retention of configuration.[20−23] Actually, however, it is controlled largely by the structure of **12** which undergoes hydride transfer with cis stereochemistry. The hydrogenolysis of resulting **13** limits the turnover rate of the steady-state catalytic cycle. The major and minor enantiomers are formed by the same mechanism involving diastereomeric intermediates. This view is supported by the following experimental observations.

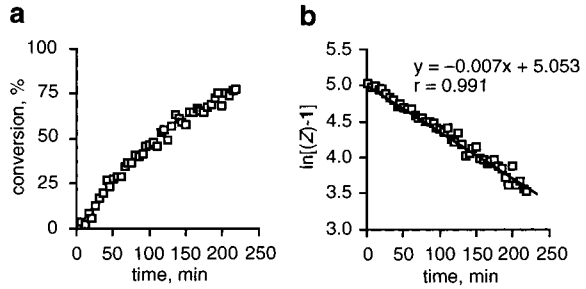

Figure 4. Time-conversion curve (a) and the first-order plot (b) for hydrogenation of (*Z*)-**1** in methanol containing (*S*)-**10**. Conditions: $[(Z)\text{-}\mathbf{1}]_0$ = 150 mM, $[(S)\text{-}\mathbf{10}]_0$ = 0.75 mM, 1 atm H_2, 30 °C.

Kinetics. The rate of hydrogenation of (*Z*)-**1** with (*S*)-**10** in methanol under 1 atm of H_2 at 30 °C was measured by using a Teflon-coated hydrogenation vessel. The reaction was monitored by the intensity of the IR carbonyl stretching band of **2** at 1750 cm^{-1}. Figure 4a shows the time-conversion curve obtained under the conditions of the initial concentrations, $[(Z)\text{-}\mathbf{1}]_0$ = 150 mM and $[(S)\text{-}\mathbf{10}]_0$ = 0.75 mM. Plots of $\ln[(Z)\text{-}\mathbf{1}]_t$ versus time are reasonably linear with a coefficient correlation value of 0.991 (Figure 4b), indicating a pseudo-first-order dependence on the enamide concentration in the reaction system.[40,41] Therefore, the rate is described simply by the rate law $-d[(Z)\text{-}\mathbf{1}]/dt = k_{obs}[(Z)\text{-}\mathbf{1}]$, where k_{obs} is 6.7×10^{-3} min^{-1}.

(36) The cationic analogue of **13** is reported by Bergens, see ref 22.
(37) (a) van der Schaaf, P. A.; Kolly, R.; Hafner, A. *Chem. Commun.* **2000**, 1045−1046. (b) Huang, D.; Folting, K.; Caulton, K. G. *J. Am. Chem. Soc.* **1999**, *121*, 10318−10322. (c) Huang, D.; Streib, W. E.; Bollinger, J. C.; Caulton, K. G.; Winter, R. F.; Scheiring, T. *J. Am. Chem. Soc.* **1999**, *121*, 8087−8097.
(38) (a) Huang, D.; Koren, P. R.; Folting, K.; Davidson, E. R.; Caulton, K. G. *J. Am. Chem. Soc.* **2000**, *122*, 8916−8931. (b) Yamakawa, M.; Ito, H.; Noyori, R. *J. Am. Chem. Soc.* **2000**, *122*, 1466−1478. (c) Schanz, H.-J.; Jafarpour, L.; Stevens, E. D.; Nolan, S. P. *Organometallics* **1999**, *18*, 5187−5190. (d) Shen, J.; Haar, C. M.; Stevens, E. D.; Nolan, S. P. *J. Organomet. Chem.* **1998**, *571*, 205−213. (e) Ogasawara, M.; Huang, D.; Streib, W. E.; Huffman, J. C.; Gallego-Planas, N.; Maseras, F.; Eisenstein, O.; Caulton, K. G. *J. Am. Chem. Soc.* **1997**, *119*, 8642−8651.
(39) (a) Feiken, N.; Pregosin, P. S.; Trabesinger, G.; Scalone, M. *Organometallics* **1997**, *16*, 537−543. (b) Feiken, N.; Pregosin, P. S.; Trabesinger, G.; Albinati, A.; Evoli, G. L. *Organometallics* **1997**, *16*, 5756−5762. (c) den Reijer, C. J.; Wörle, M.; Pregosin, P. S. *Organometallics* **2000**, *19*, 309−316.
(40) Under the conditions of <0.7-atm H_2 partial pressure, $[(Z)\text{-}\mathbf{1}]_0$ = 200 mM, and $[(S)\text{-}\mathbf{10}]_0$ = 1.0 mM, the first-order plot of the time-conversion curve deviates from the linearity, probably due to the mass transfer problem, see refs 30, 31. k_{obs} at 0.33 atm of H_2 under the standard condition was obtained at 10% conversion.
(41) With a pressure higher than 7 atm, the reaction follows zero-order kinetics in $[(Z)\text{-}\mathbf{1}]_t$, indicating the operation of a different mechanism at higher pressure.

Because the conversion of (*S*)-**10** to **11** is controlled only by acid/base thermodynamics[32,33] and is independent of hydrogen pressure under the standard conditions[42] as judged by NMR (vide infra), the total concentration of the Ru hydride species, either active or inactive, is constant.

$$[\mathbf{11}] = a[(S)\text{-}\mathbf{10}]_0 \quad (1)$$

The rate law was derived by using eq 1, the rate constant k_1 for the intramolecular hydride transfer, **11** → **13**, the rate constant k_{-1} for the β-elimination, **13** → **11**, k_2 for the hydrogenolysis, **13** → **11**, and k_3 for the methanolysis, **13** → **14**. Under this steady-state condition, the rates of formation and consumption of **13** are identical, establishing the equations, $k_1[\mathbf{11}][(Z)\text{-}\mathbf{1}] = k_{-1}[\mathbf{13}] + k_2[\mathbf{13}][H_2] + k_3[\mathbf{13}][CH_3OH]$. Because the rate of conversion of enamide is estimated by that of the turnover-limiting step, $-d[(Z)\text{-}\mathbf{1}]/dt$ can be expressed by $k_2[\mathbf{13}][H_2] + k_3[\mathbf{13}][CH_3OH]$, the mathematical modification of which leads to $-d[(Z)\text{-}\mathbf{1}]/dt = k_1[\mathbf{11}][(Z)\text{-}\mathbf{1}](k_2[H_2] + k_3[CH_3OH])(k_{-1} + k_2[H_2] + k_3[CH_3OH])^{-1}$. Substitution of [**11**] by $a[(S)\text{-}\mathbf{10}]_0$ affords the following rate law.

$$-d[(Z)\text{-}\mathbf{1}]/dt = ak_1[(S)\text{-}\mathbf{10}]_0[(Z)\text{-}\mathbf{1}](k_2[H_2] + k_3[CH_3OH])(k_{-1} + k_2[H_2] + k_3[CH_3OH])^{-1} \quad (2)$$

Providing the proposed rate equation with experimental confirmation, the effects of $[(S)\text{-}\mathbf{10}]_0$, hydrogen pressure ($[H_2]$), $[(Z)\text{-}\mathbf{1}]_0$, $[(S)\text{-}\mathbf{2}]_0$, and $[CH_3COOH]$ on the rate were examined. The rate of conversion of (*Z*)-**1** to (*S*)-**2** was measured as a function of $[(S)\text{-}\mathbf{10}]_0$ ranging from 0.1 to 1.0 mM. For each reaction, a good pseudo-first-order relation was obtained by plotting $\ln[(Z)\text{-}\mathbf{1}]_t$ versus time (Figure 4). A plot of the rate constant versus $[(S)\text{-}\mathbf{10}]_0$ established a first-order dependence of the rate of conversion of (*Z*)-**1** to (*S*)-**2** on $[(S)\text{-}\mathbf{10}]_0$ (Figure 5a). The $\ln[(Z)\text{-}\mathbf{1}]_t$-time correlation curves obtained by changing $[H_2]$ also gave pseudo-first-order relations. As shown in Figure 5b, at H_2 pressures between 0.6 and 1.2 atm, the rates were followed under first-order kinetics, consistent with the mechanism that **13** → **11** is turnover-determining.[40] With a pressure higher than 1.5 atm, the linearity was lost, probably due to the change in mechanism from monohydride to polyhydride[32,33] or the coexistence of the two mechanisms. The contamination of the less enantioselective polyhydride pathway is minimal, if any, at 0.6−1.2 atm.

Figure 5c and d shows the effects of the substrate and product. The rate of hydrogenation was markedly decreased with an increase in the initial substrate concentration from 100 to 200 mM, while an excellent pseudo-first-order relation was obtained in this concentration range (see Supporting Information, Figure S-2). With a concentration higher than 200 mM, the hydrogenation rate was gradually decreased and reached a constant level (Figure 5c). The reaction obeyed near zero-order kinetics in the product concentration added to the reaction system (Figure 5d). As shown in Figure 5e, the addition of CH_3COOH in an even 15 equiv quantity to Ru did not affect the rate of the hydrogenation. Thus, the Ru-catalyzed hydrogenation of (*Z*)-**1** follows first-order kinetics in the concentration of (*Z*)-**1** in the reaction system, initial concentration of (*S*)-**10**, and hydrogen pressure, indicating that k_{-1} must be larger than $k_2[H_2] + k_3[CH_3OH]$ in eq 2. The β-elimination occurs easily at the rate of eq 3. NMR spectra of reaction mixture under catalytic conditions showed solvated (*S*)-**10** as the only detectable Ru-containing species (vide infra).

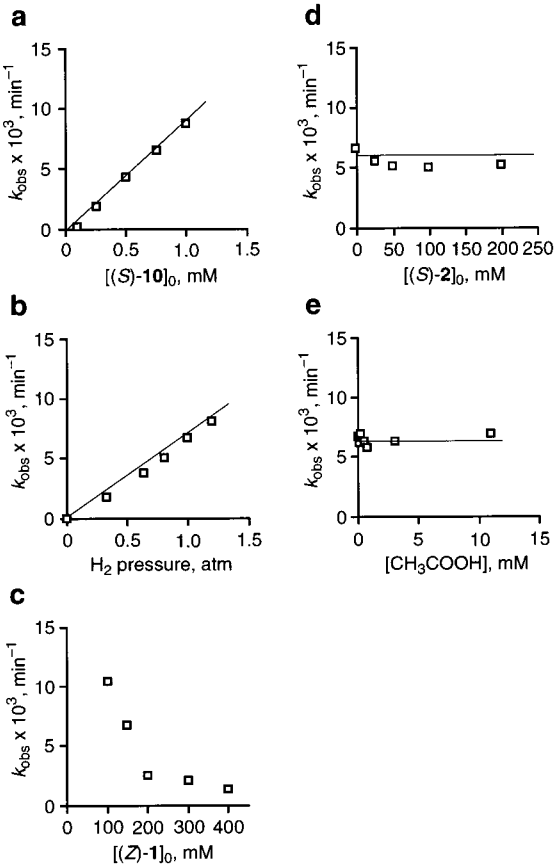

Figure 5. Dependence of $[(S)\text{-}\mathbf{10}]_0$, H_2 pressure, $[(Z)\text{-}\mathbf{1}]_0$, $[(S)\text{-}\mathbf{2}]_0$, and $[CH_3COOH]$ on the rate constant k_{obs} in hydrogenation of (*Z*)-**1** in CH_3OH at 30 °C. (a) Plots of k_{obs} as a function of $[(S)\text{-}\mathbf{10}]_0$ ($[(Z)\text{-}\mathbf{1}]_0 = 150$ mM, 1.0 atm H_2). (b) Plots of k_{obs} as a function of H_2 pressure ($[(Z)\text{-}\mathbf{1}]_0 = 150$ mM, $[(S)\text{-}\mathbf{10}]_0 = 0.75$ mM). (c) Plots of k_{obs} as a function of $[(Z)\text{-}\mathbf{1}]_0$ ($[(S)\text{-}\mathbf{10}]_0 = 0.75$ mM, 1.0 atm H_2). (d) Plots of k_{obs} as a function of $[(S)\text{-}\mathbf{2}]_0$ ($[(Z)\text{-}\mathbf{1}]_0 = 150$ mM, $[(S)\text{-}\mathbf{10}]_0 = 0.75$ mM, 1.0 atm H_2). (e) Plots of k_{obs} as a function of $[CH_3COOH]$ ($[(Z)\text{-}\mathbf{1}]_0 = 150$ mM, $[(S)\text{-}\mathbf{10}]_0 = 0.75$ mM, 1.0 atm H_2).

$$-d[(Z)\text{-}\mathbf{1}]/dt = ak_1k_{-1}^{-1}[(S)\text{-}\mathbf{10}]_0[(Z)\text{-}\mathbf{1}](k_2[H_2] + k_3[CH_3OH]) \quad (3)$$

There is seen an "apparent" contradiction between Figure 4 and Figure 5c with respect to substrate inhibition. The reaction in fact suffered from the inhibitory effect of (*Z*)-**1** as shown in Figure 5c. Because the rate was unaffected by the structurally similar α-ethylstyrene and methyl (*Z*)-cinnamate or the hydrogenation product **2** and many other amides, this effect would be ascribed to the formation of nonproductive RuH/enamide complexes, as suggested by the NMR study described below. Thus, an increase in [(*Z*)-**1**] retards the formation of catalytically active **11** from (*S*)-**10**, resulting in a decrease of the *a* value in eq 1. This process, however, is kinetically separated from the catalytic cycle in which **11** is not poisoned by (*Z*)-**1**, as indicated by the time/ln[(*Z*)-**1**] relation in Figure 4b. Consequently, the turnover rate virtually exhibits a first-order relation in the whole

(42) This view agrees with the kinetic data of Halpern in hydrogenation of tiglic acid.[20] k_{obs} of the hydrogenolysis of Ru(RCOO)(tiglato)(binap) is calculated to be 45×10^{-3} min^{-1} which is 1 order of magnitude larger than k_{obs} of the hydrogenation of (*Z*)-**1**.

Table 1. Analysis of *S*-Enriched Product **2** Obtained by Isotope-Labeling Experiments Using (*Z*)-**1** and (*S*)-**10**[a]

	conditions		
	HD in CH_3OD	H_2 in CH_3OD	D_2 in CH_3OD
% enantiomeric excess[b]	92	90	91
protium incorporation, %			
H in C(2)	41	84	0.5
H in C(3)	57	98	0.9
product distribution, %			
(*S*)-**2**-*h*,*h*	23	79	<1
(*R*)-**2**-*h*,*h*	0.8	3	0
(*S*)-**2**-*d*,*h*	33	14	<1
(*R*)-**2**-*d*,*h*	0.6	1.5	0
(*S*,*S*)-**2**-*h*,*d*	16	2	<1
(*R*,*R*)-**2**-*h*,*d*	1.2	0.4	0
(*S*,*S*)-**2**-*d*,*d*	21	0.4	88
(*R*,*R*)-**2**-*d*,*d*	0.9	0.1	3
(*S*)-**2**-*d*,d_2	3	0	5
(*R*)-**2**-*d*,d_2	0.5	0	1

[a] Reactions were carried out at 1 atm under the standard conditions. The detailed procedures for the reaction and analysis are described in the Experimental Section. Solvent CH_3OD contains 0.5% CH_3OH. HD gas contains 2% H_2 and 2% D_2. D_2 gas contains 0.4% HD. In all cases, the *S**,*R** diastereomers were not detected. [b] The ee was determined by HPLC analysis.

concentration range (Figure 5c and Figure S-2 in Supporting Information). This indicates that the rate of conversion from the nonproductive RuH/enamide complexes to the reactive **11** is slower than that of hydrogenation. The effect of substrate concentration is not yet fully explained, but the kinetic behavior shown in Figures 4, 5c, and S-2 (Supporting Information) is consistent with the present view.

The kinetic study led us to conclude that the rate is limited by a step involving molecular hydrogen. An Arrhenius plot of the kinetic data for hydrogenation under 1 atm at 26, 30, and 36 °C provides the activation energy of $E_a = 79$ kJ mol^{-1}. Although this value is not a true activation energy but results from the combination of various kinetic and thermodynamic quantities involved in the multistep reaction, the overall value is helpful for an understanding of the energy diagram.

Isotope Labeling Patterns. The above kinetic study corroborates the catalytic cycles in Figure 3 but does not provide information about the pathway cleaving the Ru−C bond of **13**, either through hydrogenolysis or through protonolysis. Isotope labeling experiments using a deuterated gas and solvent shed light on this issue as well as on the nature of the catalytic species. The reactions using HD and H_2 were analyzed at a conversion of 7−10% to minimize the complication caused by gas/solvent and gas/gas isotope exchange. Careful GC analysis of the unreacted hydrogen using a $MnCl_2$-coated Al_2O_3 stationary phase and GC-MS analysis of the recovered solvent indicated that the initial location of the isotopes basically remains the same during the reaction. The presence of enamide substrates significantly retards the isotope exchange.[43] The extent of observed scrambling does not affect the mechanistic argument. Thus, three sets of experiments were conducted with a combination of HD/CH_3OD, H_2/CH_3OD, and D_2/CH_3OD with $[(Z)\text{-}\mathbf{1}]_0 = 150$ mM and $[(S)\text{-}\mathbf{10}]_0 = 1.0$ mM, which led to the isotopomers, (*S*)-**2**-*h*,*h*, (*S*)-**2**-*d*,*h*, (*S*,*S*)-**2**-*h*,*d*, (*S*,*R*)-**2**-*h*,*d*, (*S*,*S*)-**2**-*d*,*d*, (*S*,*R*)-**2**-*d*,*d*, (*R*)-**2**-*h*,*h*, (*R*)-**2**-*d*,*h*, (*R*,*R*)-**2**-*h*,*d*, (*R*,*S*)-**2**-*h*,*d*, (*R*,*R*)-**2**-*d*,*d*, and (*R*,*S*)-**2**-*d*,*d*, as well as triply deuterium-incorporated isotopomers, (*S*)-**2**-*d*,d_2 and (*R*)-**2**-*d*,d_2. The *S* and *R* enantiomers of **2** with ca. 90% ee were separated by preparative HPLC on a chiral stational phase and analyzed by the $^{13}C\{^1H,^2H\}$-^1H correlation NMR technique. The ratio of the five isotopomers, **2**-*h*,*h*, **2**-*d*,*h*, **2**-*h*,*d*, **2**-*d*,*d*, and **2**-*d*,d_2, was determined by detailed analysis of the proton- and deuterium-decoupled ^{13}C NMR spectra. The relative stereochemistry in **2**-*h*,*d* and **2**-*d*,*d* was determined by the $^{13}C\{^1H,^2H\}$-^1H correlation NMR analysis. The products proved to be isotopically stable under the reaction conditions. Thus, when *N*-methyl-*N*-vinylacetamide was hydrogenated in methanol containing the **2**-*d*,*d* product, deuterium atoms at C(2) and C(3) of the latter were not lost during the reaction. Table 1 summarizes the product analysis.

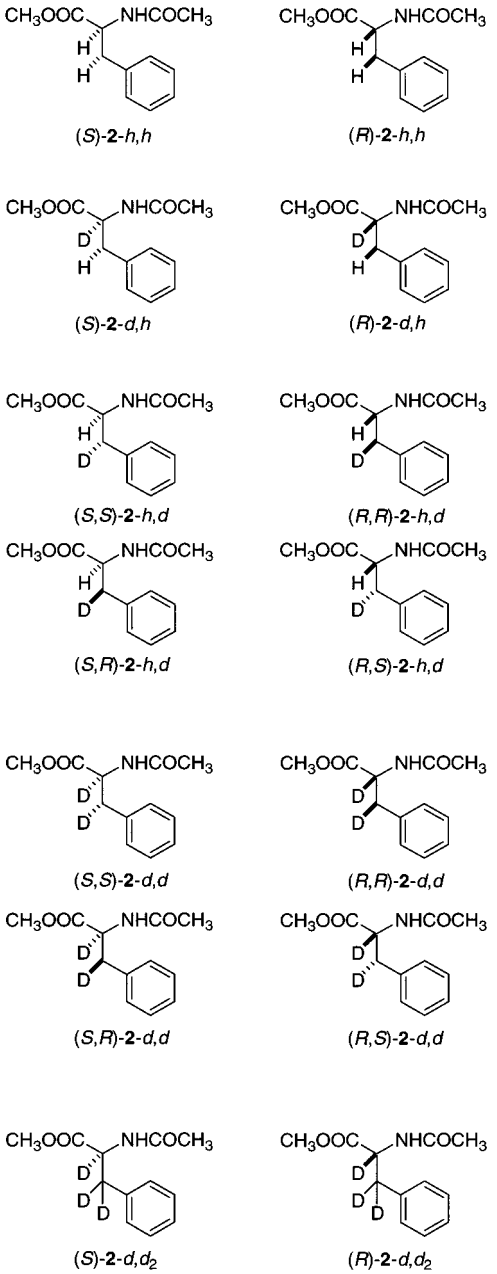

The result confirmed the operation of the monohydride mechanism with little contamination of the polyhydride mechanism, if any, under the standard conditions. Deuterium labeling

(43) This was also confirmed by reaction of 2-formyl-1-methylene-6,7-dimethoxy-1,2,3,4-tetrahydroisoquinoline with D_2 in a CH_3OH-CH_2Cl_2 mixture.

of the gas and solvent did not affect the enantioselectivity. Hydrogenation of (*Z*)-**1** in CH_3OD (99.5% pure) containing 0.67 mol % (*S*)-**10** at 30 °C under 1 atm of HD (H_2:HD:D_2 = 2:96:2) afforded, after 7% conversion, (*S*)-**2** in 92% ee, which contained 41 and 57% of the protiums in C(2) and C(3), respectively. The ratio of recovered H_2, HD, and D_2 was 6:89:5 and that of CH_3OH and CH_3OD was <1:99. The $^{13}C\{^1H,^2H\}$ NMR spectra of separated enantiomers (*S*)-**2** and (*R*)-**2** revealed that the labeled product consisted of the eight isotopomers, (*S*)-**2**-*h*,*h*, (*S*)-**2**-*d*,*h*, (*S*,*S*)-**2**-*h*,*d*, (*S*,*S*)-**2**-*d*,*d*, (*R*)-**2**-*h*,*h*, (*R*)-**2**-*d*,*h*, (*R*,*R*)-**2**-*h*,*d*, and (*R*,*R*)-**2**-*d*,*d* in a 23:33:16:21:0.8:0.6:1.2:0.9 ratio. In both *S* and *R* products, the distribution of H and D was approximately statistic. The departure from the quantitative statistics was due to the isotope effect and partial isotope exchange. Thus, the catalytic cycle turns over by the monohydride mechanism. The origin of the trideuterio products, (*S*)-**2**-*d*,d_2 (3%) and (*R*)-**2**-*d*,d_2 (0.5%), will be discussed later.

Molecular hydrogen is a major, but not the sole, hydrogen source. The reaction of (*Z*)-**1** at 1 atm of H_2 in CH_3OD gave, after 10% conversion, a mixture of (*S*)-**2**-*h*,*h*, (*S*)-**2**-*d*,*h*, (*S*,*S*)-**2**-*h*,*d*, (*S*,*S*)-**2**-*d*,*d*, and their enantiomers in a 79:14:2:0.4:3:1.5:0.4:0.1 ratio. This result indicates that the major *S* product is produced largely by hydrogenolysis of the Ru−C bond of the intermediate **13** but also by methanolysis.[44] The extent of the latter is estimated to be ca. 15% of the hydrogenolysis, and this value is significantly larger than the reported <4% in a reaction using a cationic BINAP−Ru catalyst with D_2/CH_3OH.[23] At 0.3 atm, as expected, the contribution of the protonolysis is increased up to 31%. It is known that, in the hydrogenation of α,*β*- or *β*,*γ*-unsaturated carboxylic acid with the same neutral catalyst **10**, the Ru−C bond of the intermediate is cleaved preferentially by protic agents.[20,21] The formation of small amounts of (*S*,*S*)-**2**-*h*,*d* (2%) and (*S*,*S*)-**2**-*d*,*d* (0.4%), with a deuterium atom at C(3), would be a result of an H/D exchange between the Ru hydride **11** and CH_3OD via a RuH(CH_3OD) and then Ru(CH_3O)(η^2-HD) complex.[7] The observed (*S*,*S*)-**2**-*h*,*d*/(*S*,*S*)-**2**-*d*,*d* ratio of 5 that is close to the (*S*)-**2**-*h*,*h*/(*S*)-**2**-*d*,*h* ratio of 5.6 is in accord with the exocyclic migratory insertion in **12** leading to a five-membered metallacycle. This also confirms that ca. 15% of **13** is hydrolyzed by methanol. The deuterium distribution pattern in minor (*R*)-**2** is similar to that in major (*S*)-**2**,[45] indicating that the minor enantiomer is formed basically via the same monohydride route.[46]

The reaction using D_2 and CH_3OD, which gave mostly (*S*,*S*)-**2**-*d*,*d* (91% ee) after 87% conversion, is consistent with this mechanistic scheme. The chiral product possessed an *S*,*S* (major) or *R*,*R* (minor) configuration within the error limits of NMR analysis, confirming overall cis hydrogenation. The formation of small amounts of **2**-*h*,*h*, **2**-*d*,*h*, and **2**-*h*,*d* was probably due to contamination of HD to commercial D_2 and of CH_3OH to CH_3OD solvent. The lack of protium incorporation in C(2) of the product indicates that the Ru−OCH_3 bond in **14** is cleaved only by D_2 but neither by CH_3OD nor by the methyl group of Ru−OCH_3.

The absence of (*S*,*R*)- or (*R*,*S*)-**2**-*d*,*d* in the products of the D_2/CH_3OD reaction indicates that the methanolysis route also proceeds in a cis manner. This was further confirmed by the detailed analysis of the product obtained by reaction of (*Z*)-**1**-*3*-*d* under the H_2/CH_3OD conditions. Thus, after 8% conversion, a mixture of (*S*)-**2**-*h*,*h*, (*S*,*R*)-**2**-*h*,*d*, (*S*,*R*)-**2**-*d*,*d*, (*R*)-**2**-*h*,*h*, and (*R*,*S*)-**2**-*h*,*d* was obtained in a 4:80:12:1:3 ratio. The formation of (*S*,*R*)-**2**-*d*,*d* but not (*R*,*R*)-**2**-*d*,*d* indicates that the methanolysis of the Ru−C bond of major $\mathbf{13}_R$ occurred with retention of configuration at C(2).[47]

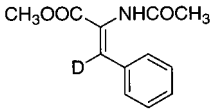

(*Z*)-**1**-*3*-*d*

The pathway forming **2**-*d*,d_2 under the HD/CH_3OD (3.5% yield) or D_2/CH_3OD (6% yield) conditions is uncertain. Formation of this minor trideuterated product tempts us to postulate the reversibility of the olefin/Ru−H insertion in **12** (Figure 3).[28] Thus, the olefinic double bond of (*Z*)-**1** is inserted into the Ru−D bond of **11** to give $\mathbf{13}_R$ with an (*R*)-$CHDC_6H_5$ group. A 120° rotation around the C(2)−C(3) bond followed by *β*-hydride elimination affords the transient RuH species containing (*E*)-**1**-*3*-*d* as a ligand. Partial or full dissociation of the olefinic ligand from Ru could take place. H/D exchange between the RuH and D_2 or CH_3OD[7] and subsequent deuteride transfer to (*E*)-**1**-*3*-*d* and deuteriolysis produces **2**-*d*,d_2. Consistent with this phenomenon, hydrogenation of (*E*)-**1** using 1 atm of D_2 and CH_3OD at 30 °C afforded, at 72% conversion, (*S*)-**2**-*d*,d_2 as a major product in 89% ee with a deuterium incorporation of 97% at C(2) and 89% (H_R) and 97% (H_S) at C(3). Unreacted (*E*)-**1** (26%) did not contain a deuterium atom, while ca. 95% of the recovered *Z* isomer (2%) was (*Z*)-**1**-*3*-*d*. This result suggests that hydrogenation of (*E*)-**1** proceeds after isomerization to (*Z*)-**1** via metallacycle **13**. However, the analysis should have been performed more cautiously, because unreacted (*Z*)-**1** (13%) and (*E*)-**1** (0.3%) recovered from the reaction of (*Z*)-**1**, using D_2 and CH_3OD, contained only <5% of the deuterium atom at C(3),[48] though **2**-*d*,d_2 was expected to form via (*Z*)-**1**-*3*-*d* or (*E*)-**1**-*3*-*d*. In a similar manner, **2**-*h*,d_2 was not detected by $^{13}C\{^1H,^2H\}$ NMR in the product formed by a reaction using HD and CH_3OD.

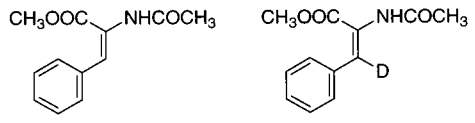

(*E*)-**1** (*E*)-**1**-*3*-*d*

Definite evidence for the reversible conversion between **11** and **13** was obtained by using the nonphenylated enamide **3** that has no *Z*/*E* problem yet readily undergoes the reverse reaction. When **3** was hydrogenated under the standard D_2/CH_3OD conditions, (*S*)-**4** (85% ee) consisting of the *d*,*d*, *d*,d_2, and *d*,d_3 isotopomers was obtained in a 71:7:22 ratio together with

(44) The point is significantly different from the reaction using a cationic BINAP−Ru catalyst.[23,24]

(45) The (*R*,*R*)-**2**-*h*,*d*/(*R*,*R*)-**2**-*d*,*d* and (*R*)-**2**-*h*,*h*/(*R*)-**2**-*d*,*h* ratios were 4 and 2, respectively. The difference is within limits of accuracy of the NMR measurement in view of the small quantities of these minor enantiomers.

(46) The minor enantiomer in BINAP−Ru-catalyzed hydrogenation of geraniol[17] is derived via a very different mechanism, see: Sun, Y.; LeBlond, C.; Wang, J.; Blackmond, D.; Laquidara, J.; Sowa, J. R., Jr. *J. Am. Chem. Soc.* **1995**, *117*, 12647−12648.

(47) Methanolysis of minor $\mathbf{13}_S$ with an (*R*)-$CHDC_6H_5$ group would produce (*R*,*S*)-**2**-*d*,*d* and/or (*S*,*S*)-**2**-*d*,*d*. Neither isomer could be observed because of the limit of ^1H NMR signal detection.

(48) A small amount of (*E*)-**1** detected may have been formed by an insignificant, minor pathway.

other isotopomers containing protium at C(2) after 94% conversion. The recovered olefin (6%) was a mixture of **3** (55%), (*Z*)-**3**-*3*-*d* (18%), (*E*)-**3**-*3*-*d* (17%), and **3**-*3*,*3*-d_2 (10%). The tri- and tetradeuterated products **4**-*d*,d_2 and **4**-*d*,d_3 (total 29%) resulted from the reversible olefin/Ru−D migratory insertion in the intermediate. Lowering the hydrogen pressure from 1 to 0.3 atm increased the amounts of the tri- and tetradeuterated compounds from 29 to 47% owing to the enhanced β-elimination/Ru−C cleavage ratio. The significant H/D exchange in the recovered olefin and excessive deuterium incorporation into the product confirmed the reversibility of the **11** → **13** step and also the exocyclic migratory insertion. This would also be the case with (*Z*)-**1**, but the reaction occurs largely without a C(2)−C(3) bond rotation.[44] A related catalytic hydrogenation of (*Z*)-**1** with a *cationic* BINAP−Ru complex using D_2 and acetone or CH_3OH does not produce **2**-*d*,d_2, the dideuterated compound **2**-*d*,*d* being the sole product, while the stoichiometric reaction suggested the rapid insertion/β-elimination equilibrium.[23]

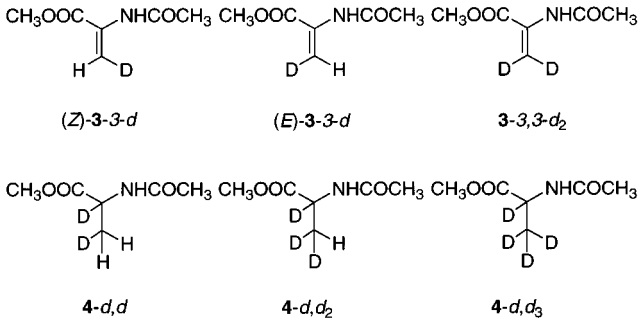

Thus, because of the monohydride-unsaturate mechanism, the newly incorporated hydrogen at C(3) originates from gaseous hydrogen and the C(2) hydrogen largely from another hydrogen molecule[28] and partly from the hydroxy proton of CH_3OH (ca. 6:1).[44] This is in strong contrast to the Rh-catalyzed hydrogenation that involves the pairwise introduction of two protiums from a single hydrogen molecule to C(2) and C(3).[5g,49]

Gas/Solvent and Gas/Gas Isotope Scrambling. The BINAP−Ru complex (*S*)-**10** not only hydrogenates (*Z*)-**1** but also catalyzes the hydrogen exchange between hydrogen molecules and between H_2 and CH_3OH. We believe that the gas/solvent exchange occurs in a RuH/CH_3OH complex, **11**(CH_3OH), via a Ru(CH_3O)(η^2-H_2) complex and that the gas/gas exchange occurs in a RuH(η^2-H_2) complex, **11**(H_2).[33] Table 2 lists the results of H/D exchange experiments using H_2/CH_3OD and HD/CH_3OD. In all cases, the recovered solvent contained >99% of CH_3OD.

Independent experiments showed that the TOF (turnover frequency defined as mols product/mol (*S*)-**10** per h) of hydrogenation of (*Z*)-**1** and gas/solvent and gas/gas isotope exchange was 5−8, 750, and >500 h^{-1}, respectively. The rate of the isotope exchange, however, was highly influenced by the coexisting compounds. Under the hydrogenation conditions, the TOF of H_2/CH_3OD scrambling was reduced to only 1 h^{-1}, 8 times lower than that of hydrogenation. Similarly, the presence of (*Z*)-**1** lowered the TOF of scrambling of HD gas to ca. 20 h^{-1}, but this rate was still 4 times higher than that of hydrogenation.

(49) Landis, C. R.; Brauch, T. W. *Inorg. Chim. Acta* **1998**, *270*, 285−297.

Table 2. Gas/Solvent and Gas/Gas Isotope Scrambling in CH_3OD Catalyzed by (*S*)-**10** in the Presence or Absence of (*Z*)-**1**[a]

	conditions				recovered gas, %			turnover frequency, h^{-1}		
entry	substrate	gas	time, h	convn, %	H_2	HD	D_2	hydrogenation	gas/solvent	gas/gas
1	(*Z*)-**1**	H_2	2	10	99.6	0.4	0	8	1	
2	(*Z*)-**1**	HD	2	7	6	89	5	5		>20
3		H_2	0.25		75	20	5		750	
4		HD	0.25		12	61	27			>500

[a] Reactions were carried out at 1 atm and 30 °C under the standard conditions. The detailed procedures for the reaction and analysis are described in the Experimental Section. Solvent CH_3OD contains 0.5% CH_3OH. The H_2:HD:D_2 ratios of H_2 gas and HD gas used are 100:0:0 and 2:96:2, respectively. In all cases, recovered solvent showed a CH_3OD/CH_3OH ratio of >99.

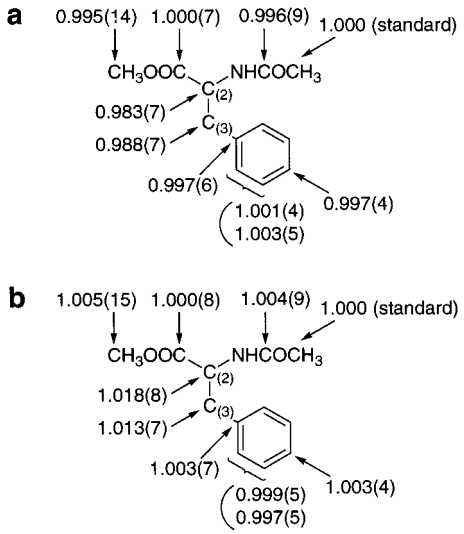

Figure 6. The ^{13}C isotopic composition of product **2** obtained at 8.28(3)% conversion (a) and the $^{12}C/^{13}C$ isotope effects (b).

Isotope Effects. The above kinetic study clearly indicates that the hydrogenolysis of the Ru alkyl **13** limits the rate of the catalytic cycle. Consistent with this view, when (*Z*)-**1** was reduced in CH_3OH under the standard conditions separately using H_2 and D_2 gas, a normal $^1H/^2H$ kinetic isotope effect of 1.2 was observed.

The $^{12}C/^{13}C$ isotope effects also agree with this mechanistic picture. Because the olefin/Ru−H migratory insertion is reversible, the repeated bond reorganization is expected to display cumulative equilibrium isotope effects at both C(2) and C(3).[50−52] In addition, it is expected that a kinetic isotope effect will be observed at C(2), because hydrogenolysis of the Ru−C(2) in **13** is turnover-limiting. Actually, the $^{12}C/^{13}C$ isotope effects at C(2) and C(3) were measured by ^{13}C NMR analysis of (*S*)-**2** in ca. 90% ee obtained at 8.28 and 100% conversions of (*Z*)-**1**. The ^{13}C signal intensities were compared between the two samples by using the acetamido $^{13}CH_3$ signal as an internal standard. As shown in Figure 6, the relative proportions of the ^{13}C isotopic composition at C(2) and C(3) were decreased by 1.7 and 1.2%, respectively. No other signals showed significant changes in the ^{13}C isotopic composition. Using the equations of Melander and Saunders,[53] the $^{12}C/^{13}C$ isotope effects are

(50) Sweany, R. L.; Halpern, J. *J. Am. Chem. Soc.* **1977**, *99*, 8335−8337.
(51) Bullock, R. M. In *Transition Metal Hydrides*; Dedieu, A., Ed.; VCH: New York, 1992; pp 263−307.
(52) Jankowski, S.; Quin, L. D.; Paneth, P.; O'Leary, M. H. *J. Am. Chem. Soc.* **1994**, *116*, 11675−11677.

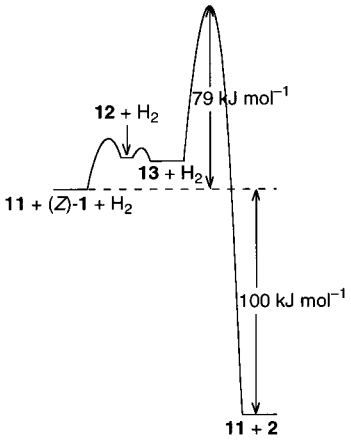

Figure 7. Energy diagram of catalytic hydrogenation.

calculated to be 1.018 at C(2) and 1.013 at C(3), respectively. If the migratory insertion in **12** were irreversible, an isotope effect is expected to be seen only at C(2). The observed isotope effects at both of the olefinic carbons are in accord with the above argument.

Energy Diagram. Figure 7 illustrates an energy diagram of the major pathway inferred from the above-described experiments. The hydrogenation of the enamide (*Z*)-**1** occurs with an exothermicity of ca. 100 kJ mol^{-1} and with an activation energy of 79 kJ mol^{-1},[54] where the hydrogenolysis of **13** is turnover-limiting. The reversibility of the process of establishing a preequilibrium, **11** + (*Z*)-**1** ⇄ **12** ⇄ **13**, has been substantiated by the isotope labeling pattern in the reaction of (*Z*)-**1** or a simpler **3** using D_2 and CH_3OD and the $^{12}C/^{13}C$ isotope effect.

The monohydride **11** is in the resting state, and the metallacycle formation is endergonic, as supported by simple mathematical analysis. If one assumes that **12** has a similar stability to **11** and is in a resting state, the relation [**11**] + [**12**] = a[(*S*)-**10**]$_0$ is established because both **11** and **12** are monohydride species. With the equilibrium constant K for **11** + (*Z*)-**1** ⇄ **12**, the rate is expressed by eq 4.

$$-\mathrm{d}[(Z)\text{-}\mathbf{1}]/\mathrm{d}t = aKk_1[(S)\text{-}\mathbf{10}]_0[(Z)\text{-}\mathbf{1}](k_2[\mathrm{H_2}] + k_3[\mathrm{CH_3OH}])(k_{-1} + k_2[\mathrm{H_2}] + k_3[\mathrm{CH_3OH}])^{-1}(1 + K[(Z)\text{-}\mathbf{1}])^{-1} \quad (4)$$

Because the catalysis in the present study follows first-order kinetics in the concentration of (*Z*)-**1** in the reaction system, an inequality K[(*Z*)-**1**] ≪ 1, [**12**] ≪ [**11**], must be satisfied. This is inconsistent with the initial assumption. In a similar manner, the assumption that **13** is in a resting state in which the energy is close to **11** + (*Z*)-**1** leads to eq 5 by use of [**11**] + [**13**] = a[(*S*)-**10**]$_0$.

$$-\mathrm{d}[(Z)\text{-}\mathbf{1}]/\mathrm{d}t = ak_1[(S)\text{-}\mathbf{10}]_0[(Z)\text{-}\mathbf{1}](k_2[\mathrm{H_2}] + k_3[\mathrm{CH_3OH}])(k_{-1} + k_2[\mathrm{H_2}] + k_3[\mathrm{CH_3OH}] + k_1[(Z)\text{-}\mathbf{1}])^{-1} \quad (5)$$

For the kinetics to be first-order in [(*Z*)-**1**], k_1[(*Z*)-**1**] must be far smaller than k_{-1}, that is, [**13**] ≪ [**11**]. This is also inconsistent with the initial condition. Actually, no Ru-alkyl species was detectable by NMR under the catalytic conditions (vide infra).[44] This is in contrast with Bergens' cationic Ru system, in which the five-membered metallacycle is more stable than the RuH catalyst + (*Z*)-**1**.[22,23] The intramolecular coordination of the ester moiety with the cationic Ru center would provide additional stability to the metallacycle intermediate.

In the present system, the minor catalytic cycle would have the same type of diagram, because the isotope labeling pattern is similar to that of the major product.

The catalytic cycle of hydrogenation of (*Z*)-**1** (Figure 3) is linked with other cycles for gas/solvent and gas/gas exchange occurring via the Ru hydride, **11**(CH_3OH) and **11**(H_2), respectively. The exchange rates are proportional to the concentrations of these RuH complexes, and the isotope exchanges between the hydride on Ru and $CH_3O\mathit{H}$ and H_2 would occur very easily when such species are formed, as seen from the high TOFs in Table 2. The presence of (*Z*)-**1** effectively prevents the gas/solvent exchange. This is *not* due to the preferential coordination of (*Z*)-**1** with **11** over CH_3OH in view of the rapid equilibrium, **11** + (*Z*)-**1** ⇄ **12** ⇄ **13**, in favor of the initial **11** + (*Z*)-**1** state. Instead, this is largely due to a high kinetic barrier for the formation of reactive **11**(CH_3OH) from **11** kinetically generated under catalytic conditions. Arrhenius analysis of the rate of H_2/CH_3OD scrambling in the presence of (*Z*)-**1** in a 26−36 °C temperature range indicated that the activation energy for the formation of **11**(CH_3OH) from **11** is 140 kJ mol^{-1}, which is unexpectedly larger than the 79 kJ mol^{-1} for hydrogenation. Thus, **11**(CH_3OH) is not involved to any great extent in the catalytic cycle of Figure 3. Rather, catalytic **11**, upon interaction with (*Z*)-**1**, enters directly into equilibration with **12**. Even if the solvento RuH species is formed, the protic ligand scarcely participates in the H/H exchange due, for example, to a *trans*-H/CH_3OH relationship or CH_3OH/OAc interligand hydrogen bonding. The methanol-free, formally unsaturated Ru complex **11** could be stabilized by extra coordination of the BINAP C(1)═C(2) bond to the Ru center.[39] Similarly, the presence of enamides lowers the degree of contribution of **11**(H_2) significantly. However, the gas/gas exchange is still faster than hydrogenation by a factor of 4 (Table 2).

Enantioface Selection. Hydrogenation of (*Z*)-**1** with the (*S*)-BINAP−Ru catalyst, (*S*)-**10**, under the standard conditions gave (*S*)-**2** and (*R*)-**2** in a 95:5 ratio. The simple derivative **3** displayed the same sense of asymmetric induction with the equal enantiomer ratio, showing that the C(3) phenyl substituent cis to the C(2) amido group does not affect the stereochemical outcome. Both (*Z*)-**1** and **3** are hydrogenated smoothly, while the reaction of (*E*)-**1** is sluggish.[44] The mechanism of Figure 3 suggests that absolute configuration of the product is determined by the first and only irreversible steps cleaving the Ru−C bond of **13**. The *S*/*R* ratio is controlled by the relative concentration of diastereomeric $\mathbf{13}_R$ and $\mathbf{13}_S$ and their reactivities toward H_2 (major) or CH_3OH (minor). Because these diastereomers would have a similar reactivity to H_2 and also CH_3OH, as judged by the structural resemblance,[4,55] the $\mathbf{13}_R/\mathbf{13}_S$ ratio becomes the

(53) Melander, L.; Saunders, W. H., Jr. *Reaction Rates of Isotopic Molecules*; Wiley: New York, 1980; pp 95−102.
(54) The exothermicity in hydrogenation of methyl *trans*-cinnamate to methyl 3-phenylpropionate is 101 kJ mol^{-1}, see: *Kagaku Binran, Ohyoukagakuhen II*, 5th ed.; The Chemical Society of Japan, Ed.; Maruzen: Tokyo, 1995; p 304.
(55) Only a very little difference is seen in the reductive elimination rates between the corresponding five-membered organorhodium hydride complexes.

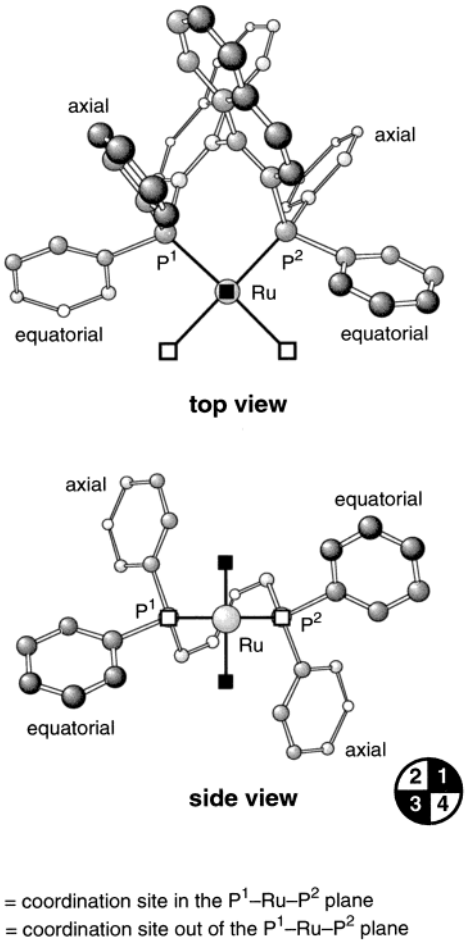

Figure 8. Chiral environment of an (*S*)-BINAP−Ru complex. The binaphthyl skeleton is omitted in the side view.

dominant factor. We postulate that this ratio (ΔG = 7.5 kJ mol^{-1}) is determined by relative stabilities of the prior diastereomeric complexes $\mathbf{12_{Re}}$ and $\mathbf{12_{Si}}$.[28,56]

An (*S*)-BINAP−Ru chiral template is schematically illustrated in Figure 8. The C_2 chiral circumstance of (*S*)-BINAP defines the chiral arrangement of the four P-phenyl substituents and of the four coordination sites shown by boxes □ and ■. The ■ sites are shielded by the axial phenyl substituents, and the □ sites significantly suffer from the steric effects of the equatorial phenyl rings. Such spatial prerequisites result in two different spatial circumstances as represented by the quarter circle in the side view. The first and third quadrants are sterically congested, while the second and fourth quadrants are relatively uncrowded. The out-of-plane ■ sites accommodate relatively small ligands such as dihydrogen, solvent molecules, hydride and other anions, whereas the bulky bidentate enamide substrate tends to occupy the in-plane □ sites so as to minimize the unfavored nonbonded repulsion with the equatorial phenyl rings. Thus, the two possible diastereomeric structures, $\mathbf{12_{Re}}$ and $\mathbf{12_{Si}}$, shown in Figure 9 are conceived for **12** in the hydrogenation of (*Z*)-**1**. Note that these reactive complexes leading smoothly to the five-membered metallacycles **13** have a parallel Ru−H/C(2)═C(3) arrangement. It is obvious that the *S*-generating structure $\mathbf{12_{Re}}$ is favored over the *R*-generating structure $\mathbf{12_{Si}}$ that has the COOR^1 group in

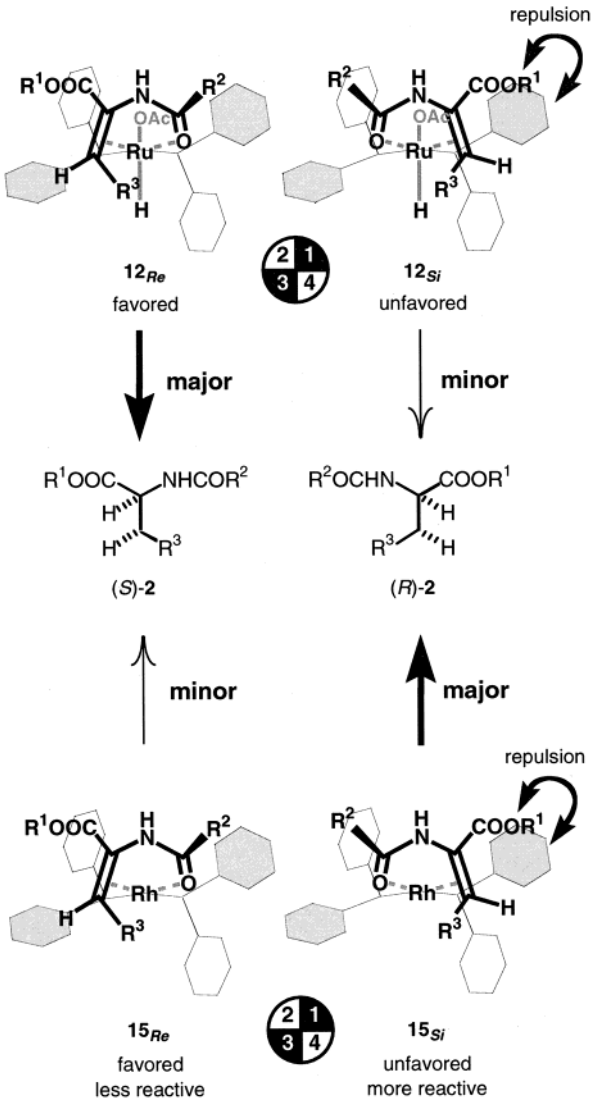

Figure 9. Enantioface selection of (*Z*)-**1** with (*S*)-BINAP−Ru(II) and (*S*)-BINAP−Rh(I) templates (side views). The binaphthyl rings are omitted for clarity.

the sterically crowded first quadrant. In $\mathbf{12_{Re}}$, the ester group is accommodated in the uncrowded second quadrant, and the N-acyl group is distant from the P-phenyl in the first quadrant. The direction of asymmetric hydrogenation is simply determined by the relative stabilities of these diastereomers ($\mathbf{12_{Re}} > \mathbf{12_{Si}}$), which are equally reactive, because the Ru centers already possess hydride to be delivered to the olefinic ligand. The same argument can safely apply to the reaction of the simple substrate **3**, for which the phenyl group in $\mathbf{12_{Re}}$ and $\mathbf{12_{Si}}$ is replaced by a hydrogen atom. Thus, this stereocomplementary model consistently explains the sense of asymmetric induction, *S* to *S* or *R* to *R*, of the BINAP−Ru-catalyzed hydrogenation of enamides.[14,15] This model also explains the lower reactivity of (*E*)-**1**, which is not readily accommodated in the BINAP−Ru template.

For square-planar (*S*)-BINAP−Rh complexes, as illustrated in Figure 9, $\mathbf{15_{Re}}$ is more stable than $\mathbf{15_{Si}}$ for the same reason.[57] However, the less stable $\mathbf{15_{Si}}$ is more reactive toward H_2 as

(56) This view is consistent with the fact that a high enantioselectivity is achieved with sterically more demanding dehydro amino phosphonic acids and 1-benzylidene tetrahydroisoquinoline substrates.[14a,c,15]

(57) For the molecular structure of Rh(binap)(norbornadiene), see: Toriumi, K.; Ito, T.; Takaya, H.; Souchi, T.; Noyori, R. *Acta Crystallogr*. **1982**, *B38*, 807−812.

observed earlier by Halpern and Brown[4g,5j,34,35a,58] and as analyzed by Brown, Bosnich,[35] and Landis.[10,59] The process involves the oxidative addition of H_2 to **15** to give the octahedral RhH_2 species **16**, followed by exo C═C/Rh−H migratory insertion and reductive elimination. The generation of the *R*-forming dihydride $\mathbf{16_{Si}}$ from minor $\mathbf{15_{Si}}$ is kinetically[35] and thermodynamically favored over the formation of the *S*-directing diastereomer $\mathbf{16_{Re}}$, which suffers the P-phenyl/COOR[1] repulsion. Thus, the extent of the contribution of major $\mathbf{15_{Re}}$ to hydrogenation is much less than its equilibrium concentration. This effect results in a dramatic reversal of the sense of asymmetric induction between the Ru and Rh catalysis using the same BINAP chirality as shown in Figure 2. This trend has been seen in the hydrogenation of many other enamide substrates,[3,14,25] albeit with some exceptions.[60] The behavior of C_2 chiral CHIRAPHOS can be interpreted in the same manner.[8a,62]

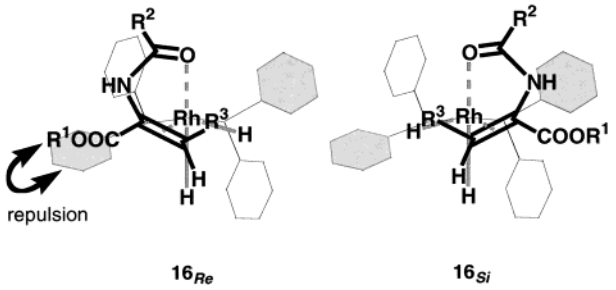

Structural Information. Catalysis is a kinetic phenomenon. The mechanistic profile of Figure 3 and the energy diagram of Figure 7 are based largely and also properly on the kinetic study, rate law analysis, isotope effects measurement, and isotope labeling experiments. These studies, however, gave no structural insights into the reactive intermediates. Structural characterization of catalytically significant complexes is generally difficult,[63] and isolable or detectable species are often kinetic repositories of species equilibrating with or derived from the real catalytic intermediates. The Ru intermediates **11**−**13** on the principal reaction coordinate (Figure 3) are short-lived, present only in low concentrations, and equilibrating with one another. Under the actual catalytic conditions, none of these intermediates were detected by NMR techniques. The only observable species was the solvated catalyst precursor (*S*)-**10**. As described below, certain complexes could be isolated or characterized by adding donor compounds or lowering temperatures, but such actions significantly perturb the real catalytic cycles. Therefore, overinterpretation based on structural information from such NMR studies as well as X-ray crystallographic analysis must be avoided. The following spectroscopic studies, coupled with the above kinetic and isotope labeling experiments, revealed that the properties of stoichiometrically and thermodynamically derived Ru complexes are significantly different from those of the kinetically generated metastable species given in Figure 3. In fact, most spectroscopically observable Ru complexes, even some solvento complexes, are not directly involved in the catalytic cycle but are derived therefrom. They are mere side products that act as reservoirs of real catalytic complexes or even retard the hydrogenation reaction.

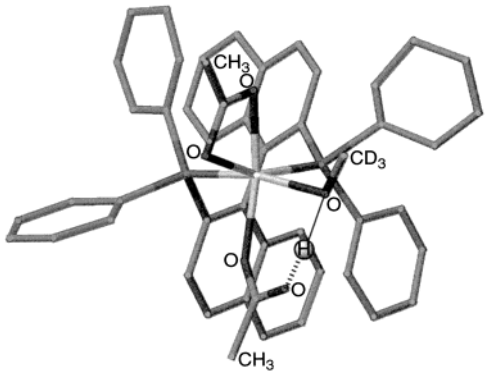

Figure 10. Molecular structure of $Ru(CH_3COO)_2(CD_3OH)$[(*S*)-binap] [(*S*)-**10**(CD_3OH)] in a crystalline state. The dotted line from H shows a supposed hydrogen bond.

Although (*S*)-**10** has C_2 symmetry in the solid state,[64] the symmetry is lost in the solution. The $^{31}P\{^1H\}$ NMR in CD_3OD (5 mM) at 23 °C showed a singlet at δ 65.7. The ^{31}P spectrum at −80 °C, however, gave the signals at δ 66.7 and 67.2 with an AB pattern (J = 45.9 Hz), and ^1H NMR in CD_3OD at −80 °C showed the acetate methyl singlets at δ 1.60 and 1.68. The nonequivalency of the two phosphorus nuclei and acetate ligands at low temperatures is ascribed to the cleavage of the acetate four-membered ring, resulting in the mono-methanol complex (*S*)-**10**(CH_3OH) (Figure 10).[20] The geometrical fixation of the bis-methanol complex via selective internal hydrogen bonding is also possible. Crystalline (*S*)-**10**(CD_3OH) was isolated and characterized by X-ray study. The methanol occupies one of the in-plane □ sites (Figure 8) and is hydrogen-bonded to the carbonyl oxygen of the monodentate acetate ligand in the out-of-plane ■ site.[65] Addition of 20 equiv of the enamide (*Z*)-**1** or **3** to a solution of (*S*)-**10**(CH_3OH) in methanol at −60 °C did not form any enamide chelate complexes, as revealed by the fact that $^{31}P\{^1H\}$ NMR gave only an AB quartet at δ 66.4 and 67.1. Therefore, if any olefin π-complexes are formed under catalytic conditions, it is probably a process after the formation of Ru hydrides that parallels the cycle in Figure 3.

When a pale yellow 5 mM solution of (*S*)-**10** in methanol containing 10 equiv of DMF was allowed to stand at 24 °C, the solvento Ru monohydride, **11**(CH_3OH), was formed slowly.[67] This solvento complex may act as a reservoir of the actual catalytic species **11** to some extent. The $^{31}P\{^1H\}$ NMR spectrum of **11**(CH_3OH) in a homogeneous solution at 24−25 °C showed a characteristic AB pattern at δ 77.5−77.8 and 83.7−84.2 with $J_{P,P}$ = 50.4 Hz.[68] These ^{31}P signals have cross-peaks with the proton signal at δ −20.4 (t, $J_{H,P}$ = 33.3 Hz) in the ^{31}P-^1H

(58) Bender, B. R.; Koller, M.; Nanz, D.; von Philipsborn, W. *J. Am. Chem. Soc.* **1993**, *115*, 5889−5890.
(59) Landis, C. R.; Feldgus, S. *Angew. Chem., Int. Ed.* **2000**, *39*, 2863−2866.
(60) Hydrogenation of dimethyl 1-(formamido)ethenylphosphonate with [Rh[(*S*)-binap]$(CH_3OH)_2$]ClO_4 gave the corresponding (*R*)-α-amino phosphonate in 51% ee[61] with the same sense of asymmetric induction as observed with (*S*)-**10**.[15] Note that in going from the carboxylate to the phosphate, the *R*/*S* nomenclature is reversed due to the change in the atom priority. (*R*)-Amino phosphonic acids correspond formally to natural (*S*)-amino acids.
(61) Unpublished result.
(62) James, B. R.; Pacheco, A.; Rettig, S. J.; Thorburn, I. S.; Ball, R. G.; Ibers, J. A. *J. Mol. Catal.* **1987**, *41*, 147−161.
(63) For full structural elucidation of catalytic intermediates in asymmetric hydrogenation, see: (a) Halpern, J. In *Asymmetric Synthesis*; Morrison, J. D., Ed.; Academic Press: New York, 1985; Vol. 5, Chapter 2. (b) Haack, K.-J.; Hashiguchi, S.; Fujii, A.; Ikariya, T.; Noyori, R. *Angew. Chem., Int. Ed. Engl.* **1997**, *36*, 285−288.
(64) Ohta, T.; Takaya, H.; Noyori, R. *Inorg. Chem.* **1988**, *27*, 566−569.
(65) This O−H···O hydrogen bond is considered to be almost linear as judged by the distance between the two oxygen atoms (2.452 Å).[66]
(66) Steiner, Th.; Saenger, W. *Acta Crystallogr.* **1992**, *B48*, 819−827.
(67) In the absence of DMF, the Ru complex tends to precipitate probably due to the formation of hydride-bridged polymers.

heteronuclear correlated spectrum taken at −60 °C. The small $J_{H,P}$ value is characteristic of the hydride cis to the two phosphorus atoms. The triplet signal of the hydride was broadened at 24 °C both in the absence and in the presence of 1 atm of H_2, indicating an equilibrium with Ru polyhydride species such as a trihydride or an η^2-H_2 coordinated RuH complex.[32,33] The hydride signal was decreased upon exposure to D_2 gas. This complex may be responsible for the slower, less enantioselective reaction under a high hydrogen pressure. The yield of **11**(CH_3OH) is increased to 30% by decreasing the concentration of (*S*)-**10** to 0.75 mM in CH_3OH containing a 10 mol amount of DMF. Thus, CH_3OH can act as a hydride source, but molecular hydrogen accelerates the monohydride formation. In actual hydrogenation, the hydride source is H_2 and not methyl in CH_3OH.

A stoichiometric model reaction of (*S*)-**10** and H_2 in the absence of enamides suggests that the concentration of RuH species is not affected by hydrogen pressure in a range from 0.35 to 1.2 atm under the conditions of $[(S)\text{-}\mathbf{10}]_0 = 0.75$ mM, [DMF] = 7.5 mM, CH_3OH, and 30 °C, although some polyhydrides may be formed under high pressure. Instead, the acidity/basicity of the reaction system controls the quantity of the RuH species. The conversion of (*S*)-**10**, determined by $^{31}P\{^1H\}$ NMR after a 1 h reaction, remained constant at 51−56%. This result supports the postulate that the [H_2] term in the rate eq 3 is involved only in the hydrogenolysis rate of **13** but not in the formation of **11** from **10**.[42] Addition of an excess of acetic acid (up to 15−20 equiv) to a solution of **10** in CH_3OH did not change the quantity of the hydride species, whereas upon addition of a 10 mol amount of triethylamine or 1,8-bis(dimethylamino)naphthalene (proton sponge), **11**(CH_3OH) was formed quantitatively. The heterolysis of H_2 with (*S*)-**10** proceeds via a significantly acidic η^2-H_2 Ru complex formulated as (*S*)-**10**(H_2).[32,33] Therefore, in the presence of a sufficient amount of H_2 in the homogeneous phase, the equilibrium quantity of the RuH species is limited by the basicity of solution. Under basic conditions, this was the case even without H_2, giving **11**(CH_3OH) quantitatively after 2 h. The same RuH species was formed even in CD_3OH. Thus, addition of an excess amount of CD_3OH to the RuD species which had been prepared in CD_3OD generated the RuH species, as judged by ^1H NMR. The RuD intermediate undergoes hydrogen exchange with a methanol proton and a hydrogen molecule under certain conditions. In the absence of an enamide substrate, such hydrogen exchange occurs rapidly in the ^1H NMR time scale, giving a broad hydride signal at 24 °C. In the catalytic system, however, **11**(CH_3OH) does not exist in view of the lack of hydrogen exchange. Thus, **11**(CH_3OH) behaves differently from catalytically active **11**.[39]

When one molar amount of triphenylphosphine was added to a methanol solution of (*S*)-**10** under 1 atm of H_2, RuH(CH_3COO)[(*S*)-binap]P(C_6H_5)$_3$ (**17**) was formed quantitatively. The NMR spectra in Figure 11 confirmed the octahedral structure in which the hydride occupies the coordination site cis to the three *mer*-arranged phosphorus atoms. The ^1H NMR in toluene-d_8 exhibited a characteristic hydride signal at δ −17.8 with a ddd pattern with $J_{H,P}$ = 29.0, 25.3, and 23.5 Hz, while the $^{31}P\{^1H\}$ NMR in toluene-d_8 showed three different phosphorus signals at δ 40.5 (dd, $J_{P,P}$ = 299.3 and 23.7 Hz), 49.0 (dd, $J_{P,P}$ = 299.3 and 38.5 Hz), and 82.8 (dd, $J_{P,P}$ = 38.5 and 23.7 Hz). The stereochemistry was confirmed by an X-ray diffraction study of structurally similar RuH(*t*-C_4H_9COO)[(*S*)-binap]P(C_6H_5)$_3$ (**18**) (Figure 12). The triphenylphosphine-complexed RuH species, though less active than **11**, effected the hydrogenation of (*Z*)-**1** under the standard conditions (1 atm, 30 °C) to give (*S*)-**2** in 82−83% ee in 40 (pivalate) to 75% conversion (acetate) after 24 h.

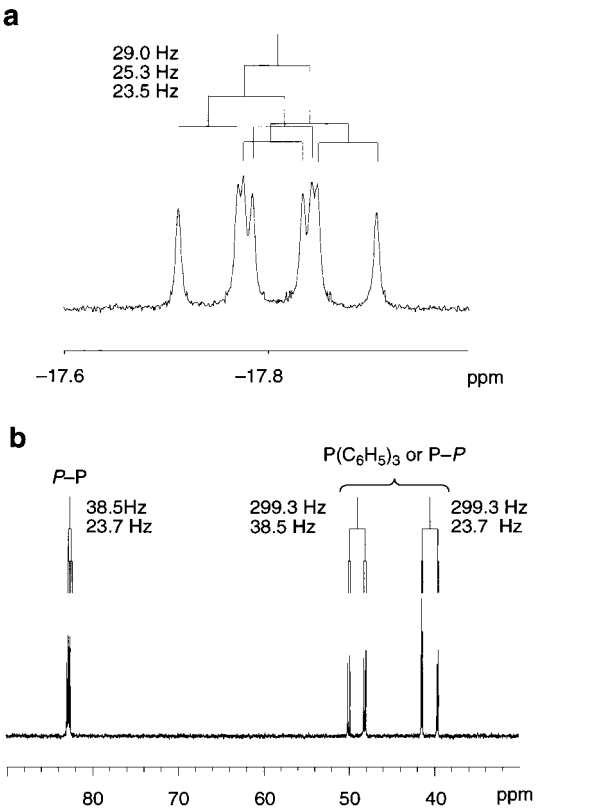

Figure 11. Hydride region of ^1H NMR spectrum (a) and $^{31}P\{^1H\}$ NMR spectrum (b) of a 10 mM solution of RuH(CH_3COO)[(*S*)-binap]P(C_6H_5)$_3$ (**17**) in toluene-d_8 at 25 °C. P−P = (*S*)-BINAP.

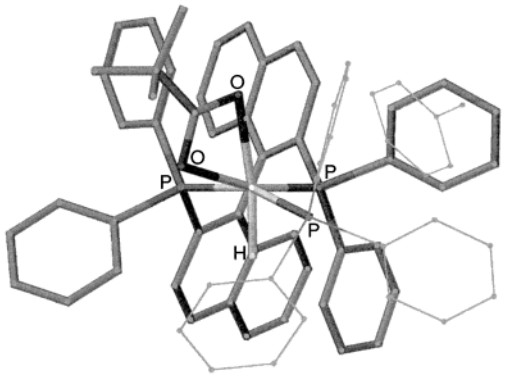

Figure 12. Molecular structure of RuH(*t*-C_4H_9COO)[(*S*)-binap]P(C_6H_5)$_3$ (**18**) cocrystallized with toluene.

With the confirmation of Ru hydride formation from (*S*)-**10** and H_2,[69] we examined the behavior of the BINAP−Ru complexes in the presence of an enamide (*Z*)-**1** or **3**. Figure 13 illustrates the change in $^{31}P\{^1H\}$ NMR spectra of the Ru complexes. Figure 13a and b shows the spectra of an initial

(68) Two additional doublet signals **x** emerged at δ 52.1 and 52.5 with $J_{P,P}$ = 47.5 Hz. The signal intensity increased to up to 15% of that of (*S*)-**10** when the reaction was performed at 24 °C for 48 h under 1 atm of H_2 in methanol containing a 10 mol amount of DMF per (*S*)-**10**. These signals are unassignable at this moment.

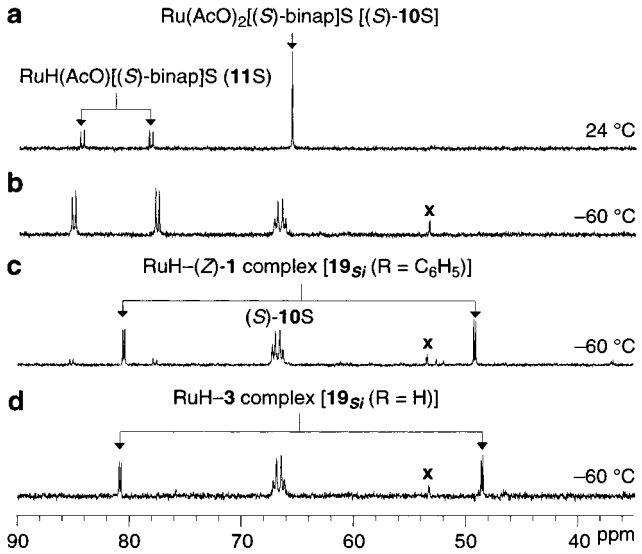

Figure 13. The $^{31}P\{^1H\}$ NMR spectrum change in the BINAP−Ru-catalyzed hydrogenation of (*Z*)-**1** and **3**. S = CH_3OH or CD_3OH. (a) Spectrum at 24 °C after 20 h exposure of (*S*)-**10** (5 mM) to 2 atm of H_2 at 24 °C. (b) Spectrum of the solution in stage a at −60 °C. (c) Spectrum at −60 °C after addition of (*Z*)-**1** into the solution in stage a at −78 °C. (d) Spectrum at −60 °C after addition of **3** into the solution in stage a at −78 °C. The conditions are the same as those in c.

CH_3OH-CD_3OH solution of the methanol-complexed (*S*)-**10** and **11** (ca. 1:1) and the mixture containing DMF under 1 atm of H_2 taken at 24 and −60 °C, respectively. Figure 13c is the spectrum obtained by addition of a 20 mol amount of (*Z*)-**1**, where hydrogenation conditions are mimicked. An unassignable AB quartet centered at δ 52.1 and 52.5 is marked with an **x**.[68] At −60 °C, most signals of solvento **11** disappeared, and two new doublet signals appeared at δ 49.2 and 80.5 ($J_{P,P}$ = 26.7 Hz) (Figure 13c).[70]

The new ^{31}P doublet signals have cross-peaks with the proton signal at δ −18.9 (dd, $J_{H,P}$ = 31.4 and 27.5 Hz). The fluxional structures of the Ru diacetate (*S*)-**10** were frozen at the low temperature, giving an AB quartet at δ 66.4 and 67.1. Separately, ^1H NMR at this stage showed that ca. 10% of (*Z*)-**1** had been converted to (*S*)-**2**. The new compound was apparently not a simple σ-bonded enamide or product complex. All of the ^{31}P splitting pattern, high chemical shifts, and NMR behavior of Figure 13 suggest the formation of a RuH−enamide chelating complex. Although it is highly tempting to interpret this as direct evidence of **12$_{Re}$**,[24] we believe that this was due to a nonproductive RuH−enamide complex that may or may not act as a catalyst reservoir depending on reaction conditions. For the enamide C(2)═C(3) bond to undergo a smooth migratory insertion into the Ru−H linkage, these bonds are required to be cis and parallel, as seen in **12$_{Re}$** and **12$_{Si}$** in Figure 9. These geometrically well-aligned RuH species are invisible by means of NMR at or even below the hydrogenation temperature due to the lower stability or the equilibration with **13**. On the other hand, the stereoisomers incapable of giving **13** would be

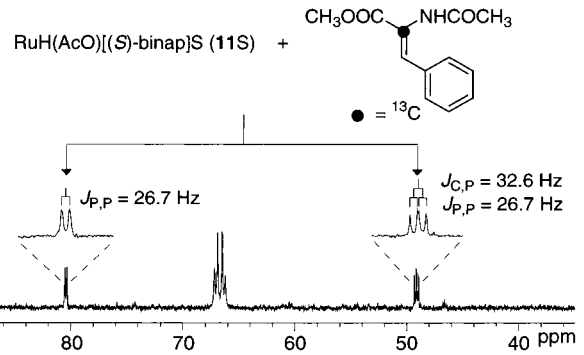

Figure 14. $^{31}P\{^1H\}$ NMR spectrum of the RuH−substrate complex **19$_{Si}$** (R = C_6H_5) obtained with (*Z*)-**1**-*2*-^{13}C in a 4:1 CH_3OH-CD_3OH mixture containing DMF (50 mM) at −60 °C. S = CH_3OH or CD_3OH.

detectable. The complexes **19** (R = C_6H_5), which have a near-perpendicular Ru−H/C(2)═C(3) and parallel Ru−OAc/C(2)═C(3) geometry, are the candidates. The diastereomers possessing a perpendicular Ru−H/C(2)═C(3) but antiparallel Ru−OAc/C(2)═C(3) alignment are unlikely to be candidates owing to the nonbonded repulsion between the P-phenyl rings and the C(3)HR group. Thus, we propose the octahedral structure **19$_{Si}$**, which is more favorable than the **19$_{Re}$** involving P-phenyl/$COOCH_3$ repulsion. Such a mode of enamide coordination is important in the reactive RhH_2 intermediate **16** in the related Rh-catalyzed hydrogenation of Figure 1.[35] In fact, the $^{31}P\{^1H\}$ NMR study using ^{13}C-labeled enamides corroborates this view. With (*Z*)-**1**-*2*-^{13}C, as illustrated in Figure 14, the ^{31}P signal at δ 49.2 was split into a doublet of doublet with $J_{P,P}$ = 26.7 Hz and $J_{C,P}$ = 32.6 Hz, while the signal pattern at δ 80.5 did not change.[28] The signal at δ 49.2 was assignable to the phosphorus atom trans to the chelating C═^{13}C double bond. In addition, the perpendicular geometry was supported by the observation of an nOe between the closely located Ru*H* and enamide C(3)*H*. Actually, −7% enhancement of the C(3) proton signal at δ 1.4 (br s) was seen when the hydride signal at δ −18.9 was selectively enhanced with a GOESY sequence.[28,71,72] In addition, the complex obtained with (*Z*)-**1**-*1′*-^{13}C did not exhibit any long-range coupling between the acetamido ^{13}C═O signal and the ^{31}P signal pair at both δ 49.2 and δ 80.5.[44] This is different in the case of [RuH[(*R*)-binap]((*Z*)-**1**)(CH_3CN)]BF_4.[24] Overall, the NMR investigation supports the structure **19$_{Si}$** (R = C_6H_5) but not the reactive **12$_{Re}$** or **12$_{Si}$**. The observed nOe also excludes the possibility of **20$_{Re}$** or **20$_{Si}$** (R = C_6H_5) with an antiparallel Ru−H/C(2)═C(3) alignment. These stereoisomers should be formed at such a low temperature, because (1) the intermolecular olefin complexation/decomplexation process is frozen, (2) the structures are very similar to **12$_{Re}$** or **12$_{Si}$**, and (3) the endo migratory insertion is kinetically unfavored.[10] However, these stereoisomers are NMR-invisible probably due to the facile intramolecular conversion[73] to the parallel isomers **12** equilibrating with **13**. When a solution of stage c in Figure 13 was warmed and allowed to stand at 23 °C for 24 h, the signal due to **19$_{Si}$** (R = C_6H_5) completely disappeared because all of (*Z*)-**1**

(69) For relevant Ru-diphosphine monohydride complexes, see: (a) Currao, A.; Feiken, N.; Macchioni, A.; Nesper, R.; Pregosin, P. S.; Trabesinger, G. *Helv. Chim. Acta* **1996**, *79*, 1587−1591. (b) Wiles, J. A.; Lee, C. E.; McDonald, R.; Bergens, S. H. *Organometallics* **1996**, *15*, 3782−3784. (c) Mezzetti, A.; Costella, L.; Del Zotto, A.; Rigo, P.; Consiglio, G. *Gazz. Chim. Ital.* **1993**, *123*, 155−164. (d) Kawano, H.; Ishii, Y.; Komada, T.; Saburi, M.; Uchida, Y. *Chem. Lett.* **1987**, 1311−1314.

(70) Addition of a 10 mol amount of (*Z*)-**1** gave a 3:7 mixture of **11**(CH_3OH) and the new compound.

(71) GOESY = gradient enhanced nuclear Overhauser effect spectroscopy.

(72) Stonehouse, J.; Adell, P.; Keeler, J.; Shaka, A. J. *J. Am. Chem. Soc.* **1994**, *116*, 6037−6038.

(73) (a) Brown, J. M.; Chaloner, P. A.; Morris, G. A. *J. Chem. Soc., Perkin Trans. 2* **1987**, 1583−1588. (b) Bircher, H.; Bender, B. R.; von Philipsborn, W. *Magn. Reson. Chem.* **1993**, *31*, 293−298. (c) Kadyrov, R.; Freier, T.; Heller, D.; Michalik, M.; Selke, R. *J. Chem. Soc., Chem. Commun.* **1995**, 1745−1746. (d) Ramsden, J. A.; Claridge, T. D. W.; Brown, J. M. *J. Chem. Soc., Chem. Commun.* **1995**, 2469−2471.

had been transformed to **2**. Thus, this nonproductive Ru complex existed as long as (*Z*)-**1** remained in the reaction system, but when all the substrate was consumed, it returned to **11**(CH_3OH). Finally, it was converted to a RuH complexed with the benzene ring of **2**,[22,74] at least under the conditions of the NMR study.

The nonphenylated enamide **3** behaves similarly at −60 °C. ^{31}P NMR in Figure 13d suggests the formation of the RuH−enamide chelating complex $\mathbf{19_{Si}}$ (R = H).

These results suggest that, under the catalytic conditions, original **10** is distributed mostly to **10**(CH_3OH), nonproductive **19**, and catalytic RuH **11**. **11**(CH_3OH) is absent as far as (*Z*)-**1** exists. The NMR study coupled with kinetic experiments indicate that reaction of **11**(CH_3OH) and enamide is largely nonproductive but interaction between methanol free **11** and enamide is productive. This is well understood, when one assumes that (1) η^2-acetate to η^1-acetate change in hexacoordinate **11**(CH_3OH), generating a pentacoordinate RuH with an out-of-plane vacant site, is easier than dissociation of CH_3OH, (2) catalytic **11** possesses an in-plane vacant site, and (3) enamide chelate complexation starts with the amide C═O coordination.[73] The conversion from **19** to **11** is virtually irreversible under the standard hydrogenation conditions.[75] Although the turnover-limiting step is the hydrogenolysis of the metallacycle **13** (Figure 3), this species was undetectable by NMR because of the equilibration with a thermodynamically favored mixture of **11** and the free enamide via **12**.[44]

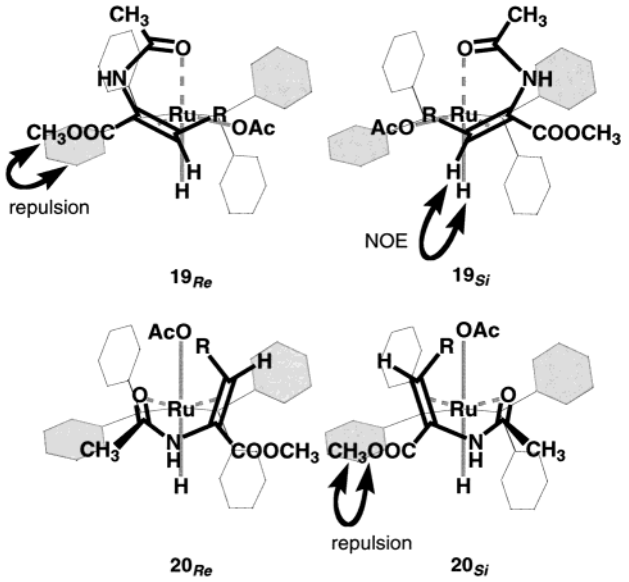

Conclusion

The profile of the asymmetric hydrogenation of enamides catalyzed by BINAP−Ru diacetate is different in many respects from the well-studied Rh(I)-catalyzed reaction that proceeds via an unsaturate-dihydride mechanism.[4,5] The BINAP−Ru-catalyzed reaction occurs via a monohydride-unsaturate pathway.[15,23] Both major and minor enantiomers are formed by the same mechanism. A Ru monohydride species is first generated from the diacetate and H_2 with the liberation of acetic acid and then forms a short-lived enamide complex which delivers the hydride to the C(3) position. The addition of the RuH species to the olefinic bond is endergonic and reversible.[44] The Ru−C bond of the resulting five-membered metallacycle is cleaved largely by H_2[28] and partly by protic CH_3OH, both with retention of configuration to give a cis-dihydrogenation product and revive the RuH species. Consequently, the Ru-catalyzed hydrogenation incorporates two protiums into enamides from two different donor molecules. The overall rate is limited by the Ru−C hydrogenolysis step.[28] The enantioselection is made during this irreversible step but actually is controlled by the relative free energies of the diastereomeric RuH/olefin complexes. The sense of asymmetric induction is opposite to that of the hydrogenation using Rh(I) complexes with the same BINAP ligand[3,14,25] and is explained in terms of the stereocomplementary models of the RuH/enamide complexes. The monohydride mechanism operates only in a low-pressure hydrogenation. Increasing the hydrogen pressure induces a different, probably polyhydride, mechanism. The detection of true catalytic Ru complexes is difficult. Most spectroscopically observable complexes are not directly involved in the catalytic cycle.

Experimental Section

General. Infrared (IR) spectra were recorded on a Shimadzu DR-8000 spectrometer and were expressed by wavenumber (cm^{-1}). Nuclear magnetic resonance (NMR) spectra were measured on a JEOL JNM-A400 equipped with a pulsed field gradient unit and a triple-resonance probe, a JEOL JNM-ECP500, JEOL JNM-ECP800, or Varian INOVA-500 instrument. The chemical shifts are expressed in parts per million (ppm) downfield from $Si(CH_3)_4$ or in ppm relative to $CHCl_3$, CH_3OH, DMSO, benzene, and toluene (δ 7.26, 3.30, 2.50, 7.16, and 2.09 in ^1H NMR and δ 77.0, 49.0, 39.5, 128.0, and 20.4 in ^{13}C NMR). All chemical shifts of $^{31}P\{^1H\}$ NMR spectra are reported downfield in ppm relative to external 85% H_3PO_4 at 0.00 ppm. Signal patterns of ^1H NMR as well as $^{31}P\{^1H\}$ NMR are indicated as follows: s, singlet; d, doublet; t, triplet; q, quartet; m, multiplet; br, broad signal. X-ray crystallographic analyses were conducted on a Rigaku RAXIS IV imaging plate area detector equipped with a liquid nitrogen cryostat. Optical rotation was measured on a JASCO DIP-1000 digital polarimeter using a sodium lamp in a 5 mm × 10 cm cell. GC-MS analyses were performed using a Shimadzu QP-5000. Electrospray ionization-time-of-flight ESI-TOFMS was performed using a PE Biosystems Mariner. All melting points were determined on a Yanaco melting point apparatus and were uncorrected. Elemental analyses were performed on a LECO-CHN 900 instrument.

Analytical thin-layer chromatography (TLC) was performed using Merck 5715 indicating plates precoated with silica gel 60 F254 (layer thickness 0.25 mm). The product spots were visualized with a solution of *o*-anisaldehyde. Liquid chromatographic purification was performed by flash column chromatography using glass columns packed with Merck 9385 (230−400 mesh). HPLC analyses were conducted on a Shimadzu LC-6A instrument equipped with a RHEODYNE 7125 injector and a Shimadzu SPD-6A UV detector. For preparative HPLC, a Shimadzu LC-10AD instrument was used and was equipped with a system controller SCL-10A, a degasser DGU-4A, an autosampler SIL-10AXL, a fraction collector GILSON MODEL 201, and a Shimadzu SPD-10A UV detector. DAICEL CHIRALCEL OD was used as a

(74) Mashima, K.; Kusano, K.; Ohta, T.; Noyori, R.; Takaya, H. *J. Chem. Soc., Chem. Commun.* **1989**, 1208−1210.

(75) The nonproductive complex **19** is convertible to catalytic **11** but only slowly. In fact, some nonlinearity was observed in the time/ln[(*Z*)-**1**] relation at a low and high initial concentration of (*Z*)-**1** (see Supporting Information, Figure S-2). The slight downward deviation with $[(Z)\text{-}\mathbf{1}]_0 = 100$ mM can be ascribed to a gradual increase in [**11**]. Plots for a higher initial concentration of (*Z*)-**1** (400 mM), on the other hand, show a slight upward deviation. This is probably due to the low substrate conversion during which the nonproductive **19** is still generating, but not to slow irreversible loss of catalyst activity. Actually, the catalytic activity in reaction of **3** was recovered upon renewal of the enamide substrate. Because the **19** → **11** conversion is slower than that of hydrogenation, the extent of the deviation was small. Under the standard conditions, straight lines were obtained. We appreciate the valuable suggestion of referees in this regard.

column packed with a chiral stationary phase. The eluted compounds were detected at 254 nm light. For recycling preparative HPLC, a Japan Analytical Industry Model LC-908 instrument was used.

All manipulations in the BINAP−Ru-catalyzed hydrogenation were carried out by using the usual Schlenk technique on a dual manifold vacuum-Ar system. Operational processes basically followed the previously reported ones.[14,15] The structure of (*Z*)-**1** was determined by X-ray crystallographic analysis. For details, see Supporting Information. The structures of hydrogenation products **2** and **4** were determined by comparing the spectral data with the reported values.[8c,9a] The ee's of **2** and **4** were determined by HPLC and GC analysis, respectively. HPLC conditions were as follows: column, CHIRALCEL OD (4.6 mm × 25 cm); eluent, a 9:1 hexane−2-propanol mixture; flow rate, 1 mL min^{-1}; temperature, 30 °C; detection, 254 nm light; retention time (t_R) of (*S*)-**2**, 13.0 min; t_R of (*R*)-**2**, 9.9 min. GC conditions: capillary column, Chrompack XE-60-(*S*)-valine-(*S*)-phenylethylamide on WCOT fused silica (0.25 mm × 50 m); column temperature, 140 °C; injection and detection temperature, 180 °C; carrier gas, He; flow rate, 118 kPa; split ratio, 40:1; t_R of (*R*)-**4**, 14.0 min; t_R of (*S*)-**4**, 14.7 min. The absolute configurations for **2** and **4** were determined by comparing the sign of optical rotations with the reported values.[8c,9a]

Materials. CH_3OH, CH_3OD, CD_3OH, and CD_3OD for hydrogenation and NMR studies were degassed at the refluxing temperature in the presence of Mg (250 mg/100 mL) under an Ar stream for 6 h and distilled into Schlenk flasks. CH_3OD contains 0.5% OH species. The solvent was degassed by three freeze−thaw cycles before hydrogenation. In a similar manner, toluene and hexane were distilled from Na benzophenone ketyl. DMF was distilled from molecular sieves 4A. Toluene-d_8 available from Aldrich was distilled over a Na−K alloy. $CDCl_3$, C_6D_6, and DMSO-d_6 were purchased from Aldrich and used without further purification. Triphenylphosphine and 1,8-bis(dimethylamino)naphthalene were obtained from nacalai tesque. Paraformaldehyde-d_2 was purchased from Aldrich. For kinetic study, acetic acid of a guaranteed grade available from nacalai tesque was distilled from anhydrous $CuSO_4$ (500 mg/100 mL) under an Ar stream and diluted with CH_3OH to an 11 mM solution. Triethylamine was purchased from nacalai tesque and distilled from CaH_2 (3 g/L) under an Ar stream.

Ar gas (99.998%) was purified by being passed through a column of the BASF catalyst R3-11 at 80 °C and then through a column of granular $CaSO_4$. H_2 gas of a 99.99999% grade, D_2 gas containing 0.4% of HD, a 1:1 mixture of H_2 (99.99999%)−Ar gas, a 1:5.7 mixture of H_2−Ar gas, and a 1:5.7 mixture of D_2 (99.7%)−Ar gas were purchased from Nippon Sanso, and HD gas containing 2% H_2 and 2% D_2 was obtained from Isotec. These gases were used for hydrogenation without purification. Ne and He gases for GC analysis of the H_2/HD/D_2 ratio were obtained from Takachiho Kogyo and the Japan Helium Center, respectively. The purity of Ne was 99.999%. He gas of a 99.9999% purity, which was purchased from Nippon Sanso, was used for GC-MS analysis of the CH_3OH/CH_3OD ratio. CO gas of a 99.95% grade was obtained from Nippon Sanso and used without purification.

$Ru(CH_3COO)_2$[(*S*)-binap] [(*S*)-**10**] was prepared by a previously reported method.[76]

The enamide substrates, (*Z*)-**1**,[77] (*E*)-**1**,[8c] (*Z*)-**1**-*3*-*d*,[78] (*E*)-**1**-*3*-*d*,[78] (*Z*)-**1**-*2*-^{13}C,[77] (*Z*)-**1**-*1′*-^{13}C,[78] and **3**-*3*,*3*-d_2[78], were prepared according to the known methods. These experimentals are described in Supporting Information. The enamide **3**, commercially available from Tokyo Kasei, was purified by recrystallization from a 3:1 hexane−ether mixture (mp 50.5−52.0 °C (lit:[79] mp 52−54 °C)). *N*-Methyl-*N*-vinylacetamide was purchased from Aldrich and purified by distillation over molecular sieves 4A at 75 °C and 22 mmHg.

Kinetic Experiments. Kinetic investigation was carried out by use of a Teflon-coated stainless autoclave fitted with a variable temperature jacket, a magnetically controlled-mechanical stirring system, and a Ge crystal rod for total internal reflectance measurement. The figure of the apparatus is shown in Supporting Information. A typical procedure is represented as follows. The substrate (*Z*)-**1** (493 mg, 2.25 mmol) and CH_3OH (15 mL) were placed into a dry, Ar-filled 80 mL Schlenk tube. The solution was degassed by three freeze−thaw cycles and was transferred via a stainless cannula to another 80 mL Schlenk tube containing a pale brown solid (*S*)-**10** (9.5 mg, 0.011 mmol) under a slightly positive Ar pressure. After being further degassed by two freeze−thaw cycles, the yellow solution of the substrate and catalyst was introduced into the Ar-filled reactor by use of Ar pressure. The temperature of the reactor was set to 30 °C, and the whole system was allowed to equilibrate for 15 min. At this point, the IR spectrum was taken as a blank. The inner Ar gas was replaced with a 1:1 mixture of H_2−Ar gas by three pressurization−release cycles, and the partial pressure of H_2 was adjusted to 1 atm, which was maintained during the reaction by keeping the connection of the reactor to the H_2 cylinder open. Data were collected 2 min after stirring was started at 600 rpm.[30] The difference spectrum was taken every 5 min by scanning 40 times for 45 s in the band range from 400 to 4600 cm^{-1}. The measurement was continued for 220 min. The observed rate constant k_{obs} was calculated to be 6.7×10^{-3} min^{-1} on the basis of conversion and change in the area ratio of the C=O absorption band of (*S*)-**2** at 1750 cm^{-1}. The conversion was calculated, after removal of the solvent, by comparison of the ^1H NMR signal ratio at δ 3.84 (s, $COOCH_3$ of (*Z*)-**1**) and δ 3.72 (s, $COOCH_3$ of (*S*)-**2**) to be 78%. The mixture was purified by silica gel column chromatography (3 g; eluent, a 1:10 hexane−ether mixture) to give (*S*)-**2** in 90% ee and (*Z*)-**1**.

Likewise, the effects of catalyst concentration, H_2 pressure, initial concentration of (*Z*)-**1** and (*S*)-**2**, concentration of CH_3COOH, and temperature were examined. The conditions and the rate constant k_{obs} are listed in Table 3.

The reaction at 100 atm in an autoclave[76b] (88 mg of (*Z*)-**1**; [(*S*)-**10**] = 0.75 mM; [(*Z*)-**1**] = 100 mM) at 30 °C for 5 h gave (*S*)-**2** in 70% ee with 50% conversion. The result indicated that hydrogenation at 100 atm was ca. 5 times slower than that at 1 atm (see, Table 3, entry 13).

Isotope Labeling Experiments. (a) H_2/HD/D_2 Analysis. The analysis system comprised a gas-collector part, drying equipment for carrier gas, H_2/HD/D_2 separation part, FID detector, and controller. The gas-collector part was assembled by welding as much as possible to maintain a 10^{-4} mmHg order of vacuum. The sampling loop (ca. 2.9 mL) was joined to a digital pressure gauge with 0.8 mmHg accuracy to measure the amount of gas sample. A stainless column (10 mm × 1 m) packed with molecular sieves 5A (60−80 mesh) was heated at 250 °C for 6 h and used for removal of a small amount of water contained in a carrier gas. Separation of H_2, HD, and D_2 was performed on a stainless column (4 mm × 3 m) filled with 6% $MnCl_2$ on Al_2O_3.[80] The column was aged, before use, at 100 °C for 8 h under a He flow. For the connection between two columns, tabular-type but not taper-type packings were used to minimize the degree of shrinkage at low temperatures. A typical analysis procedure is described below. An 80 mL Schlenk tube with a Young's tap, which contained a gas sample, was connected to the gas collector. About 100 mmHg of gas was transferred into a sampling loop, and the gas was introduced into a GC system by an appropriate valve operation. The analysis conditions were as follows: column temperature, −196 °C; injection temperature, 40 °C; detection temperature, 100 °C; carrier gas, Ne; column head pressure, 0.5 kg cm^{-2}. The retention times of H_2, HD, and D_2 were 6.4, 7.6, and 9.4 min with peak widths of 0.90, 0.83, and 1.66 min, respectively, indicating that the degree of separation was enough for

(76) (a) Kitamura, M.; Tokunaga, M.; Noyori, R. *J. Org. Chem.* **1992**, *57*, 4053−4054. (b) Takaya, H.; Inoue, S.; Tokunaga, M.; Kitamura, M.; Noyori, R. *Org. Synth.* **1993**, *72*, 74−85.
(77) Herbst, R. M.; Shemin, D. *Org. Synth. Collect. Vol. II* **1943**, 1−3.
(78) Kober, R.; Steglich, W. *Liebigs Ann. Chem.* **1983**, 599−609.
(79) Rothstein, E. *Chem. Commun.* **1949**, 1968−1972.
(80) Kudo, H.; Fujie, M.; Tanase, M.; Kato, M.; Kurosawa, K.; Sugai, H.; Umezawa, H.; Matsuzaki, T.; Nagamine, K. *Appl. Radiat. Isot.* **1992**, *43*, 577−583.

Table 3. Kinetic Data in Hydrogenation of (*Z*)-**1** in CH_3OH Containing $Ru(CH_3COO)_2$[(*S*)-binap] [(*S*)-**10**][a]

entry	[(*S*)-**10**], mM	H_2, atm	[(*Z*)-**1**]$_0$, mM	[(*S*)-**2**]$_0$,[b] mM	[CH_3COOH], mM	temp, K	k_{obs}, min^{-1}
1	0.10	1.0	150	0	0	303	0.1×10^{-3}
2	0.25	1.0	150	0	0	303	1.9×10^{-3}
3	0.50	1.0	150	0	0	303	4.3×10^{-3}
4	0.75	1.0	150	0	0	303	6.7×10^{-3}
5	1.0	1.0	150	0	0	303	8.7×10^{-3}
6	0.75	0	150	0	0	303	0×10^{-3}
7	0.75	0.33	150	0	0	303	1.8×10^{-3}
8	0.75	0.63	150	0	0	303	3.8×10^{-3}
9	0.75	0.80	150	0	0	303	5.1×10^{-3}
10	0.75	1.2	150	0	0	303	8.2×10^{-3}
11	0.75	1.7	150	0	0	303	7.6×10^{-3}
12	0.75	3.0	150	0	0	303	8.4×10^{-3}
13	0.75	1.0	100	0	0	303	10×10^{-3}
14	0.75	1.0	200	0	0	303	2.5×10^{-3}
15	0.75	1.0	300	0	0	303	2.1×10^{-3}
16	0.75	1.0	400	0	0	303	1.3×10^{-3}
17	0.75	1.0	150	25	0	303	5.6×10^{-3}
18	0.75	1.0	150	50	0	303	5.1×10^{-3}
19	0.75	1.0	150	100	0	303	4.8×10^{-3}
20	0.75	1.0	150	200	0	303	5.3×10^{-3}
21	0.75	1.0	150	0	0.08	303	6.2×10^{-3}
22	0.75	1.0	150	0	0.15	303	6.8×10^{-3}
23	0.75	1.0	150	0	0.45	303	6.3×10^{-3}
24	0.75	1.0	150	0	0.75	303	5.5×10^{-3}
25	0.75	1.0	150	0	3.0	303	6.3×10^{-3}
26	0.75	1.0	150	0	11	303	7.0×10^{-3}
27	0.75	1.0	150	0	0	299	3.8×10^{-3}
28	0.75	1.0	150	0	0	309	10×10^{-3}

[a] All reactions were carried out in a 1.50−6.00 mmol scale. A 1:1 H_2-Ar mixture was used for the reaction at a partial H_2 pressure of 0.6−1.7 atm. A 1:3 H_2-Ar mixed gas was used for the reactions at partial H_2 pressures of 0.33 atm. For the reaction at >2.5 atm, H_2 gas was used. [b] Optically pure (*S*)-**2** was used.

quantitative analysis (see Figure S-3 in Supporting Information). The area factors of HD and D_2 for H_2 were calculated to be 0.76 and 0.59, respectively, by making a calibration curve of H_2, HD, and D_2.

(b) CH_3OH/CH_3OD Analysis. The CH_3OH/CH_3OD ratio was determined to be <1:99 by GC-MS analysis on a Shimadzu GCMS-QP5000 instrument using an *m*/*z* 15 signal of a CH_3 radical as an internal standard. GC conditions were as follows: column, CBJ-1 0.32 mm × 30 m; column temperature, 50 °C; injection temperature, 200 °C; separation temperature, 245 °C; carrier gas, 0.4 kg cm^{-2} He. MS conditions were as follows: ionization potential, 70 eV; ion source temperature, 200 °C; mass range, 35−50; scan interval, 0.5 s and simultaneous SIM detection of *m*/*z* 15, 29, 31, 32, and 33.

(c) Structural Determination of Isotopomers. The structures of the four isotopomers, **2**-*h*,*h*, **2**-*d*,*h*, **2**-*h*,*d*, and **2**-*d*,*d*, were determined by analysis of the phase-sensitive $^{13}C\{^1H,^2H\}$-^1H correlation spectrum taken in $CDCl_3$ at 23 °C using a JEOL JNM-A400 spectrometer. To minimize the magnetic field instability associated with the lack of a D-spin lock, measuring time was shortened by use of a high concentration of the sample (170 mg/0.6 mL) under the following conditions: acquisition time = 0.6701 s, pulse delay = 2.0000 s, scan number = 8, and measurement time = 50 min. The spectrum of the $^{13}C(3)$ region was shown in Figure S-4 in Supporting Information. Thus, the carbons of a mixture of the four isotopomers resonating at δ 37.33, 37.26, 37.00, and 36.92 as singlets were correlated with β-proton signals at δ 3.16 (dd, J = 14 and 6 Hz) and δ 3.06 (dd, J = 14 and 7 Hz), δ 3.15 (d, J = 14 Hz) and δ 3.05 (d, J = 14 Hz), δ 3.04 (d, J = 7 Hz), and δ 3.03 (s), respectively. Analysis of the correlation spectrum indicated that the four carbon signals were due to **2**-*h*,*h*, **2**-*d*,*h*, **2**-*h*,*d*, and **2**-*d*,*d* from a low to high field. This assignment is consistent with the empirical rule that the D-possessing carbon atom resonates in the higher field with the higher number of D.[81] The signals due to **2**-*d*,d_2 were assigned by comparison of the chemical shift of the $^{13}C(2)$ signal with that of authentic **2**-*d*,d_2 (for preparation, see Supporting Information): $^{13}C\{^1H,^2H\}$ NMR (125 MHz, $CDCl_3$) δ 53.01 (**2**-*h*,*h*), 52.96 (**2**-*h*,*d*), 52.73 (**2**-*d*,*h*), 52.68 (**2**-*d*,*d*), and 52.62 (**2**-*d*,d_2).

The signals for the isotopomers **4**-*h*,*h*, **4**-*h*,*d*, **4**-*h*,d_2, **4**-*h*,d_3, **4**-*d*,*h*, **4**-*d*,*d*, **4**-*d*,d_2, and **4**-*d*,d_3 were assigned empirically on the basis of ^{13}C NMR analysis under simultaneous irradiation of ^1H and ^2H nuclei in $CDCl_3$ at 25 °C: $^{13}C\{^1H,^2H\}$ NMR (100 MHz, $CDCl_3$) δ 47.80 (C(2) of **4**-*h*,*h*), 47.75 (C(2) of **4**-*h*,*d*), 47.70 (C(2) of **4**-*h*,d_2), 47.65 (C(2) of **4**-*h*,d_3), 47.53 (C(2) of **4**-*d*,*h*), 47.48 (C(2) of **4**-*d*,*d*), 47.43 (C(2) of **4**-*d*,d_2), and 47.37 (C(2) of **4**-*d*,d_3).

The signals for the isotopomers **3**, (*Z*)-**3**-*3*-*d*, and (*E*)-**3**-*3*-*d* were assigned empirically on the basis of $^1H\{^2H\}$ NMR analysis in $CDCl_3$ at 25 °C: $^1H\{^2H\}$ NMR (500 MHz, $CDCl_3$) δ 6.284 (s, C(3)*H*H of **3**), 6.272 (s, C(3)H of (*Z*)-**3**-*3*-*d* or (*E*)-**3**-*3*-*d*), 5.844 (d, J = 1.4 Hz, C(3)H*H* of **3**), and 5.829 (d, J = 1.4 Hz, C(3)H*H* of (*Z*)-**3**-*3*-*d* or (*E*)-**3**-*3*-*d*).

(d) Determination of the Relative Stereochemistry of 2-*h*,*d* and 2-*d*,*d*. The structure was determined by comparison of the ^1H NMR data with a known α-(acetamido)cinnamic acid.[82] ^1H NMR of synthetic (*S*)-**2**-*d*,*d* (400 MHz, DMSO-d_6): δ 2.84 (1, s, C(3)H_R). ^1H NMR of (*S*)-**2**-*h*,*h* (400 MHz, DMSO-d_6): δ 4.44 (1, ddd, J = 9.3, 7.3 and 5.4 Hz, C(2)H), 3.00 (1, dd, J = 13.7 and 5.4 Hz, C(3)H_S), 2.86 (1, dd, J = 13.7 and 9.3 Hz, C(3)H_R). This assignment was confirmed by comparison of the ^1H NMR data with those of authentic isotopomers. ^1H NMR of (*S**,*R**)-**2**-*h*,*d* (800 MHz, DMSO-d_6): δ 2.98 (1, d, J = 5.5 Hz, C(3)H_S). ^1H NMR of (*S**,*S**)-**2**-*h*,*d* (800 MHz, DMSO-d_6): δ 2.85 (1, d, J = 9.5 Hz, C(3)H_R).

(e) Separation of the Enantiomers. Major (*S*)-**2** and minor (*R*)-**2** obtained in the (*S*)-BINAP−Ru-catalyzed hydrogenation under the conditions of HD/CH_3OD, H_2/CH_3OD, and D_2/CH_3OD (vide infra) were separated under the following conditions: a mixture of (*Z*)-**1** and **2**, 10−15 mg; column, CHIRALCEL OD (20 mm × 250 mm); eluent, a 7:3 hexane−2-propanol mixture; flow rate, 6.0 mL min^{-1}; temperature, 30 °C; detection, 254 nm light; t_R of (*S*)-**2**, 26.4 min; t_R of (*R*)-**2**, 22.5 min. The degree of separation was 3.50 with the peak widths of (*R*)- and (*S*)-**2** being 0.80 and 1.6 min, respectively. Loading the sample of >25 mg on the column resulted in peak overlapping.

(f) HD/CH_3OD Conditions. The experiment with HD/CH_3OD was conducted in a 1 L Schlenk tube equipped with a Young's tap under the following conditions: reaction scale, 2.08 g of (*Z*)-**1**; [(*S*)-**10**] = 1.0 mM; [(*Z*)-**1**] = 150 mM; 1 atm of HD; CH_3OD; 30 °C. After 2 h, the gas in the reaction vessel was transferred to an 80 mL vacuumed Schlenk, and the solvent was recovered by distillation. The $H_2/HD/D_2$ and CH_3OH/CH_3OD ratios were analyzed by the above-described methods and were found to be 6:89:5 and <1:99, respectively. The TOF value of the gas/gas isotope exchange was calculated to be >20 h^{-1}. The residue was subjected to ^1H NMR and HPLC analysis, by which the conversion and ee were determined to be 7% and 92%, respectively, on the basis of the methods described in Kinetic Experiments. The crude reaction mixture was separated into crystalline (*Z*)-**1** (1.1 g) and a ca. 5:1 mixture of (*Z*)-**1** and **2** (1.0 g) by recrystallization from a ca. 1:2 hexane−ethyl acetate mixture followed by silica gel chromatography (75 g; eluent, a 1:1 hexane−ethyl acetate mixture) to remove the Ru complex. The (*Z*)-**1**/**2** mixture (22.6 mg) was separated by preparative HPLC (for conditions, see (e) Separation of the Enantiomers) to give, after 43 repetitions of the process, (*Z*)-**1** (634.8 mg), (*S*)-**2** (119.2 mg) containing (*S*)-**2**-*h*,*h*, (*S*)-**2**-*d*,*h*, (*S*,*S*)-**2**-*h*,*d*, (*S*,*S*)-**2**-*d*,*d*, and (*S*)-**2**-*d*,d_2 in a 24:34:17:22:3 ratio and (*R*)-**2** (8.3 mg) containing (*R*)-**2**-*h*,*h*, (*R*)-**2**-*d*,*h*, (*R*,*R*)-**2**-*h*,*d*, (*R*,*R*)-**2**-*d*,*d*, and (*R*)-**2**-*d*,d_2 in a 20:15:30:23:13 ratio. The isotopomer ratios were determined by measurements of the $^{13}C(3)$ signal area in the $^{13}C\{^1H,^2H\}$ NMR spectra, which were taken using a nanoprobe under the following conditions: flip angle, 63°; acquisition time (AT), 2.621 s; pulse delay

(81) Hansen, P. E. *Annu. Rep. NMR Spectrosc.* **1984**, *15*, 105−234.
(82) Detellier, C.; Gelbard, G.; Kagan, H. B. *J. Am. Chem. Soc.* **1978**, *100*, 7556−7564.

(PD), 32.379 s; sample concentration, 11.4 mg/40 μL ((*S*)-**2**) and 5.0 mg/40 μL ((*R*)-**2**); measurement time, 212 scans (2.1 h) for (*S*)-**2** and 2348 scans (6.5 h) for (*R*)-**2**. ^{1}H and ^{2}H decoupling was affected only during acquisition time. The values of relaxation time T_1 obtained by an inversion recovery method were <4.5 s for both ^{13}C(2) and ^{13}C(3) and <5 s for all protons. These values satisfied the necessary conditions, PD > 5 × T_1 of protons and AT + PD > 5 × T_1 of carbons.

(g) H_2/CH_3OD Conditions. The procedure for the H_2/CH_3OD experiment was the same as that for the HD/CH_3OD system. Reaction scale, 2.10 g of (*Z*)-**1**; [(*S*)-**10**] = 1.0 mM; [(*Z*)-**1**] = 150 mM; 1 atm of H_2; CH_3OD; 30 °C; 2 h. The conditions converted 10% of (*Z*)-**1** to give (*S*)-**2** in 90% ee (HPLC analysis). The H_2:HD:D_2 and CH_3OH:CH_3OD ratios were 99.6:0.4:0 and <1:99, respectively. The TOF value of the gas/solvent isotope exchange was calculated to be 1 h^{-1}. Recrystallization followed by silica gel column chromatography afforded a ca. 4:1 mixture of (*Z*)-**1** and **2** (1.0 g). The mixture (13 mg) was subjected to preparative HPLC, giving, after 60 repetitive injections, (*Z*)-**1** (608.3 mg), (*S*)-**2** (142.4 mg) containing (*S*)-**2**-*h*,*h*, (*S*)-**2**-*d*,*h*, (*S*,*S*)-**2**-*h*,*d*, and (*S*,*S*)-**2**-*d*,*d* in an 82.6:14.7:2.3:0.4 ratio and (*R*)-**2** (10.1 mg) containing (*R*)-**2**-*h*,*h*, (*R*)-**2**-*d*,*h*, (*R*,*R*)-**2**-*h*,*d*, and (*R*,*R*)-**2**-*d*,*d* in a 60.0:30.9:7.2:1.9 ratio. The isotopomer ratios were determined by ^{13}C{^{1}H,^{2}H} NMR analysis using a nanoprobe under the same conditions described above except for the sample concentration and measurement time. (*S*)-**2**: 16 mg/40 μL, 616 scans (6 h). (*R*)-**2**: 5.0 mg/40 μL, 1320 scans (12.8 h).

(h) D_2/CH_3OD Conditions. The procedure was the same as that for the HD/CH_3OD system except for the size of the reactor (250 mL Schlenk tube) and the purification process. Reaction scale, 362 mg of (*Z*)-**1**; [(*S*)-**10**] = 1.0 mM; [(*Z*)-**1**] = 150 mM; 1 atm of D_2; CH_3OD; 30 °C; 12 h. The conditions converted 87% of (*Z*)-**1** to (*S*)-**2** in 91% ee (HPLC analysis). The crude reaction mixture was chromatographed on silica gel (30 g; eluent, a 1:1 hexane−ethyl acetate mixture) to give a 1:9 mixture of (*Z*)-**1** and **2** (353 mg). The mixture (13 mg) was subjected to preparative HPLC, giving, after 20 repetitive injections, (*Z*)-**1** (38.4 mg) containing ca. 2% of (*E*)-**1**, (*S*)-**2** (203.0 mg) containing (*S*)-**2**-*h*,*h*, (*S*)-**2**-*d*,*h*, (*S*,*S*)-**2**-*h*,*d*, (*S*,*S*)-**2**-*d*,*d*, and (*S*)-**2**-*d*,d_2 in a <1:<1:<1:88:5 ratio and (*R*)-**2**-*d*,*d* (15.0 mg) containing (*R*)-**2**-*h*,*h*, (*R*)-**2**-*d*,*h*, (*R*,*R*)-**2**-*h*,*d*, (*R*,*R*)-**2**-*d*,*d*, and (*R*)-**2**-*d*,d_2 in a 0:0:0:3:1 ratio.

The recovered (*Z*)-**1** and (*E*)-**1** (total 34 mg) were separated by preparative HPLC (column, Develosil 100-10 (5 cm × 50 cm): eluent, a 1:1 hexane−ethyl acetate mixture containing 0.3% H_2O; flow rate, 50 mL min^{-1}) to give (*Z*)-**1** (33 mg) and (*E*)-**1** (<1 mg). The signal ratio of the vinylic proton and $COOCH_3$ in recovered (*Z*)-**1** was determined to be 1:3.0 by ^{1}H NMR analysis in C_6D_6 at 25 °C (sample concentration, 15 mM; flip angle, 45°; repetition time, 6 s; measurement time, 128 scans (12 min)). Similarly, the ratio of the vinylic proton and $COOCH_3$ in recovered (*E*)-**1** was determined to be 1:3.0.

(*E*)-**1** was deuterated under the D_2/CH_3OD conditions (reaction scale, 58.7 mg of (*E*)-**1**; [(*S*)-**10**] = 1.0 mM; [(*E*)-**1**] = 150 mM; 1 atm of D_2; CH_3OD; 30 °C; 11 h) to give a mixture of (*S*)-**2** (72%), (*E*)-**1** (26%), and (*Z*)-**1** (2%). After the crude reaction mixture was chromatographed on silica gel (7 g; eluent, a 1:10 hexane−ether mixture), the eluted product (45 mg) was subjected to preparative HPLC (column, Develosil 100-10 (5 cm × 50 cm); eluent, a 1:1 hexane−ethyl acetate mixture containing 0.3% H_2O; flow rate, 50 mL min^{-1}) to give (*S*)-**2** (30 mg) in 89% ee consisting mostly of (*S*)-**2**-*d*,d_2, (*E*)-**1** (11.8 mg) free of deuterium (<5%) at C(3), and (*Z*)-**1** (<1 mg) containing deuterium (ca. 95%) at C(3).

In a similar way, D_2/CH_3OD experiments were performed with enamide **3** under the following conditions: **3** (322 mg, 2.25 mmol); (*S*)-**10** (12.7 mg, 0.015 mmol); CH_3OD (15 mL); 1 atm of D_2; 30 °C; 33 h 20 min. The conditions converted 94% of **3** to (*S*)-**4** in 85% ee (GC analysis). The crude reaction mixture was chromatographed on silica gel (50 g; eluent, a 3:1 and then 1:3 hexane−ethyl acetate mixture) to give (*S*)-**4** (290 mg) in 85% ee consisting of **4**-*h*,*h*, **4**-*h*,*d*, **4**-*h*,d_2, **4**-*h*,d_3, **4**-*d*,*h*, **4**-*d*,*d*, **4**-*d*,d_2, and **4**-*d*,d_3 in a 0:7:5:1:4:59:6:18 ratio and recovered **3** (21 mg) containing original **3** (55%), (*Z*)-**3**-*3*-*d* (18%), (*E*)-**3**-*3*-*d* (17%), and **3**-*3*,*3*-d_2 (10%). Detection of (*Z*)-**3**-*3*-*d* or (*E*)-**3**-*3*-*d* and **3**-*3*,*3*-d_2 was carried out by means of ESI-TOFMS under the following conditions: spray tip potential, 4 kV; nozzle potential, 150 V; nozzle temperature, 150 °C; syringe pump flow rate, 2 μL min^{-1}: $[M + H]^+$ of (*Z*)-**3**-*3*-*d* or (*E*)-**3**-*3*-*d*, 145; $[M + H]^+$ of **3**-*3*,*3*-d_2, 146. When the pressure was set to 0.3 atm of D_2 under the conditions of **3** (215.1 mg, 1.50 mmol), (*S*)-**10** (8.4 mg, 9.9 μmol), CH_3OD (10 mL), 30 °C, and 81 h, the product **4** (100% conversion) in 88% ee containing these eight isotopomers in a 3:15:10:4:4:34:11:19 ratio was obtained.

(i) Isotopic Stability of 2-*d*,*d*. Hydrogenation of *N*-methyl-*N*-vinylacetamide (29 mg, 0.29 mmol) was carried out in CH_3OH (3.9 mL) containing (*S*)-**10** (3.3 mg, 3.9 μmol) and **2**-*d*,*d* containing ca. 1% proton at the C(2) and C(3) positions with an average ee of 91% (65.7 mg, 0.295 mmol) under 1 atm of H_2 at 30 °C for 24 h. The substrate was 100% converted to *N*-ethyl-*N*-methylacetamide. After removal of all the volatiles in vacuo, the residue was chromatographed on silica gel (10 g; eluent, a 1:1 hexane−ethyl acetate mixture) to give (*S*)-**2** (59 mg). Recovered **2** (5 mg) dissolved in $CDCl_3$ (0.6 mL) was subjected to ^{1}H NMR analysis at 24 °C. The intensities of C(2) and C(3) protons were virtually unchanged, indicating that **2**-*d*,*d* is isotopically stable under the reaction conditions.

(j) Stereochemistry of Methanolysis of the Intermediate 13. This procedure was the same as that for the HD/CH_3OD system except for the volume of the reactor (250 mL Schlenk tube) and the purification process. Reaction scale, 86.6 mg of (*Z*)-**1**-*3*-*d*; [(*S*)-**10**] = 1.0 mM; [(*Z*)-**1**-*3*-*d*] = 150 mM; 1 atm of H_2; CH_3OD; 30 °C; 2 h 30 min. The conditions converted 8% of (*Z*)-**1** to (*S*)-**2** in 92% ee (HPLC analysis). The H_2:HD:D_2 and CH_3OH:CH_3OD ratios were >99:<0.5:<0.5 and <1:99, respectively. The crude reaction mixture was chromatographed on silica gel (2 g; eluent, a 1:10 hexane−ether mixture) to give a 9:1 mixture of (*Z*)-**1** and **2** (79.7 mg). The mixture (64 mg) was subjected to preparative HPLC, giving (*Z*)-**1**-*3*-*d* (50 mg), (*S*)-**2** (5 mg) consisting of (*S*)-**2**-*h*,*h*, (*S*,*R*)-**2**-*h*,*d*, and (*S*,*R*)-**2**-*d*,*d* in a 4:83:13 ratio, and (*R*)-**2** (<0.5 mg) consisting of (*R*)-**2**-*h*,*h* and (*R*,*S*)-**2**-*h*,*d* in a 24:76 ratio.

(k) Isotope Exchange without (*Z*)-1. This procedure was the same as that for the HD/CH_3OD system but in the absence of (*Z*)-**1**. The reaction time and temperature were set to 15 min and 30 °C, respectively. See Table 2, entries 3 and 4. Within the range from 26 to 36 °C, the reactions were also conducted for 2 h to confirm that the TOF values of gas/solvent exchange were almost constant. In all cases, the CH_3OH:CH_3OD ratio was <1:99. At 26 °C: H_2:HD:D_2 = 6:32:64; TOF = 510 h^{-1}. At 30 °C: H_2:HD:D_2 = 12:34:54; TOF = 450 h^{-1}. At 36 °C: H_2:HD:D_2 = 6:31:63; TOF = 490 h^{-1}.

(l) Determination of the Activation Energy for the Formation of 11(CH_3OD). (*Z*)-**1** was hydrogenated under the same conditions as for the H_2/CH_3OD system for 2 h but at different temperatures. At 26 °C: H_2:HD:D_2 = 99.7:0.3:0; CH_3OH:CH_3OD = <1:99; TOF = 0.9 h^{-1}. At 36 °C: H_2:HD:D_2 = 98.4:1.6:0; CH_3OH:CH_3OD = <1:99; TOF = 5 h^{-1}. An Arrhenius plot of the TOF values at 26, 30, and 36 °C provided the activation energy of 140 kJ mol^{-1}.

Isotope Effect. (a) ^{1}H/^{2}H Kinetic Isotope Effect. This procedure was the same as that for kinetic experiments except for the kinds of gases. H_2/CH_3OH conditions: (*Z*)-**1** (493 mg, 2.25 mmol), (*S*)-**10** (9.5 mg, 0.011 mmol), CH_3OH (15 mL), 6.7 atm 1:5.7 mixture of H_2−Ar gas, 2 h, 48% conversion, 5.5 × 10^{-3} min^{-1}. D_2/CH_3OH conditions: (*Z*)-**1** (493 mg, 2.25 mmol), (*S*)-**10** (9.5 mg, 0.011 mmol), CH_3OH (15 mL), 6.7 atm 1:5.7 mixture of D_2−Ar, 2 h, 43% conversion, 4.7 × 10^{-3} min^{-1}.

(b) ^{12}C/^{13}C Isotope Effect. Hydrogenation was conducted in a 1 L Schlenk tube equipped with a Young's tap under the following conditions: reaction scale, 2.22 g of (*Z*)-**1**; [(*S*)-**10**] = 0.75 mM; [(*Z*)-**1**] = 150 mM; 1 atm of H_2; CH_3OH; 30 °C, 25 min. The residue was subjected to ^{1}H NMR and HPLC analysis, by which the conversion and ee were determined to be 8.28% and 90%, respectively, on the basis of the methods described in Kinetic Experiments. The crude

reaction mixture was purified by silica gel chromatography (75 g; eluent, a 1:1 hexane−ethyl acetate mixture) to remove the Ru complex. (*Z*)-**1** and **2** in the mixture (2.2 g) were separated by recycling preparative HPLC (column, AJ2H; eluent, $CHCl_3$; flow rate, 3.6 mL min^{-1}; detection, 254 nm light) to give (*Z*)-**1** (2 g) and (*S*)-**2** (163 mg). The product **2** obtained at 100% conversion was also prepared as a reference (about conditions, see Supporting Information). The $^{13}C\{^1H\}$ NMR signals of the two samples were compared at 125 MHz on a Varian INOVA-500 NMR under the following conditions: flip angle, 45°; points, 300 032; acquisition time (AT), 5.973 s; pulse delay (PD), 40 s; sample concentration, 160 mg/0.7 mL ((*S*)-**2**/$CDCl_3$); measurement time, 3000 scans (38 h). ^1H decoupling was affected only during acquisition time. The condition satisfied PD > 5 x T_1 of protons and AT + PD > 5 x T_1 of carbons. The measurements were performed five times for the two samples. Before collecting data, the 250 scan dummy measurements were conducted under the above conditions.

Pressure Effect on the RuH Generation. The pressure effect was investigated by use of the apparatus shown in Figure S-1 in Supporting Information. A typical procedure is represented as follows. (*S*)-**10** (9.5 mg, 0.011 mmol), DMF (8.8 μL, 0.11 mmol), and CH_3OH (15 mL) were placed into the Ar-filled reactor by use of Ar pressure. The temperature of the reactor was set to 30 °C, and the whole system was allowed to equilibrate for 15 min. The inner Ar gas was replaced with a 1:1 mixture of H_2−Ar gas by three pressurization−release cycles, and the partial pressure of H_2 was adjusted to 1.2 atm. After being stirred for 1 h, the solution was transferred via a stainless cannula to another 80 mL Schlenk tube equipped with a Young's tap by use of a 1:1 mixture of H_2−Ar gas pressure. After the solution was degassed by freeze−thaw cycles, the hydride was trapped by introducing ca. 1.5 atm of CO. After being stirred for 40 min at room temperature, the solution was concentrated to ca. 0.5 mL. To the resulting yellow solution was added CD_3OD (0.6 mL), and the aliquot was transferred to a dry NMR tube equipped with a Young's tap by use of Ar pressure. $^{31}P\{^1H\}$ NMR (162 MHz) spectrum of the mixture was taken at 25 °C. The conversion of (*S*)-**10** to the monohydride **11** was calculated to be 56% on the basis of intensities of the following signals: δ 17.48 (s, Ru(CH_3COO)$_2$(CO)$_2$[(*S*)-binap]), δ 43.63 (d, J = 29.6 Hz, RuH(CH_3COO)(CO)[(*S*)-binap]), δ 44.18 (s, RuH(CH_3COO)(CO)$_2$[(*S*)-binap]), δ 46.21 (d, J = 29.6 Hz, diastereomer of RuH(CH_3COO)(CO)[(*S*)-binap]), δ 55.60 (d, J = 29.6 Hz, diastereomer of RuH(CH_3COO)(CO)[(*S*)-binap]), and δ 62.49 (d, J = 29.6 Hz, RuH(CH_3COO)(CO)[(*S*)-binap]). The assignment of these signals was based on the literature on similar Ru hydride carbonyl complexes.[69c] Likewise, the conversions were measured by changing the partial pressure of H_2 as follows: 0 atm (1 atm of Ar), 30% conversion; 0.35 atm (1.4 atm of a 1:3 mixture of H_2−Ar), 55% conversion; 0.65 atm, 51% conversion; 1.0 atm, 56% conversion.

NMR Experiments. (a) Reaction Monitoring by NMR. The complex Ru(CH_3COO)$_2$[(*S*)-binap] [(*S*)-**10**] (2.5 mg, 3.0 μmol) was weighed into a dry NMR tube equipped with a Young's tap. The charged tube was connected to an Ar line on a dual manifold vacuum−Ar system via an adapter. The whole system was evacuated and filled with Ar gas. A 50 mM DMF solution of a 4:1 CH_3OH−CD_3OH mixture (0.6 mL) was introduced into the tube via a syringe under an Ar stream. The NMR tube was sealed by closing the Young's tap, and the mixture was agitated vigorously by an NMR tube stirrer to dissolve all the solid. The tube was then connected to a vacuum−H_2 system, and the mixture was degassed by a freeze−thaw cycle and filled with 2 atm of H_2 gas. After 20 h exposure to H_2 gas, ^{31}P and ^1H NMR spectra of the mixture were taken at 24 °C and then at −60 °C. The ^{31}P-^1H correlated NMR spectrum was also measured at this point at −60 °C. The tube was again connected to a vacuum−H_2 exchangeable line, and an enamide substrate (*Z*)-**1** or **3** (58−61 μmol) dissolved in CD_3OH (0.2 mL) was introduced at −78 °C under an H_2 stream. After the tube was sealed, the NMR experiments were performed by a gradual increase in temperature from −60 to 23 °C. The FID signals of the ^{31}P nucleus were collected at −60, −30, 0, and 23 °C, each with accumulation times of 1 h, 1 h, 30 min, and 30 min, respectively. The ^1H signals were collected at the same temperatures with accumulation times of 2−15 min. The ^{31}P-^1H correlated NMR spectrum of the mixture was taken at −60 °C. Conditions of $^{31}P\{^1H\}$ NMR: flip angle, 45°; acquisition time, 0.3375 s; pulse delay, 3.0000 s. The ^1H decoupling was affected only during acquisition time. Conditions of ^{31}P-^1H NMR: acquisition time, 0.0313−0.0527 s; pulse delay, 1.9000−2.0000 s; scan number, 80−120; measurement time, 2 h 50 min−4 h 23 min. ^{31}P and ^1H NMR of (*OC*-6-43-*C*)-[RuH(CH_3COO){(*S*)-binap}{(2,3-η-$_\kappa$O$^{1'}$)-{methyl (*Z*)-α-(acetamido)cinnamate}}] [**19$_{Si}$** (R = C_6H_5)] and (*OC*-6-43-*C*)-[RuH(CH_3COO){(*S*)-binap}{(2,3-η-$_\kappa$O$^{1'}$)-{methyl α-(acetamido)-acrylate}}] [**19$_{Si}$** (R = H)] at −60 °C are as follows. **19$_{Si}$** (R = C_6H_5): ^1H NMR (400 MHz) δ −18.9 (dd, $J_{H,P}$ = 31.4 and 27.5 Hz); $^{31}P\{^1H\}$ NMR (162 MHz) δ 49.2 (d, $J_{P,P}$ = 26.7 Hz), 80.5 (d, $J_{P,P}$ = 26.7 Hz). **19$_{Si}$** (R = H): ^1H NMR (400 MHz) δ −19.2 (t, $J_{H,P}$ = 29.3 Hz); $^{31}P\{^1H\}$ NMR (162 MHz) δ 48.7 (d, $J_{P,P}$ = 26.7 Hz), 80.8 (d, $J_{P,P}$ = 26.7 Hz). As the reaction with (*Z*)-**1** proceeded, a new pair of ^{31}P signals appeared at δ 52.5 (d, $J_{P,P}$ = 44.5 Hz) and δ 52.1 (d, $J_{P,P}$ = 44.5 Hz). The ^{31}P signals showed a cross-peak to a dd proton signal at δ −9.14 ($J_{H,P}$ = 40.3 and 29.3 Hz). Dissolution of (*S*)-**10** in a 1:1 mixture of toluene-d_8 and CD_3OH also afforded the characteristic ^{31}P signals at δ 52.6 with $J_{P,P}$ = 44.4 Hz and δ 52.1 with $J_{P,P}$ = 44.4 Hz which are correlated with the ^1H signal at δ −9.43 (dd, $J_{H,P}$ = 39.6 and 29.6 Hz). These results indicate that the signals observed with (*Z*)-**1** are assignable to the RuH compound with an η^6-benzene ring of (*Z*)-**1** and **2**.[22,74]

(b) nOe Experiment. Because the concentration of the RuH−enamide complex prepared under the H_2 atmosphere was too low to detect nOe, the experiment was carried out in the presence of a base by using an NMR tube equipped with a Young's tap. A 70 mM 1,8-bis(dimethylamino)naphthalene solution of CD_3OH (0.6 mL) was introduced into the NMR tube containing Ru(CH_3COO)$_2$[(*S*)-binap] [(*S*)-**10**] (3.5 mg, 4.2 μmol) via a syringe under an Ar stream. The tube was sealed by closing the Young's tap, and the mixture was agitated vigorously by an NMR tube stirrer to dissolve all the solid. After 2 h, the ^1H NMR spectrum of the mixture was taken at 25 °C: ^1H NMR (800 MHz) δ −20.3 (t, $J_{H,P}$ = 33.7 Hz, RuH). The conversion of (*S*)-**10** to **11**(CD_3OH) was ca. 95%. The tube was again connected to a vacuum−Ar exchangeable line, and (*Z*)-**1** (24.1 mg, 0.011 mmol) dissolved in CD_3OH (0.3 mL) was introduced to the tube at room temperature, giving four hydride species including **11**(CD_3OH) and **19$_{Si}$** (R = C_6H_5): ^1H NMR (800 MHz) δ −18.3 (dd, $J_{H,P}$ = 34.2 and 20.4 Hz), −19.0 (t, $J_{H,P}$ = 29.7 Hz, **19$_{Si}$** (R = C_6H_5)), −19.9 (t, $J_{H,P}$ = 31.5 Hz), −20.3 (t, $J_{H,P}$ = 33.7 Hz, **11**(CD_3OH)). The ratio of these species was 1:7:4:5 from the downfield. The nOe spectrum was taken by using a GOESY sequence.[71,72] The target was set to the hydride signal of **19$_{Si}$** (R = C_6H_5) at δ −19.0, and the −7% enhancement of the signal at δ 1.4 (br s) was observed. The signal at δ 1.4 disappeared under the condition using (*Z*)-**1**-*3*-*d* as substrate and CD_3OD as solvent, indicating that this signal is assignable to the olefinic proton of the coordinated (*Z*)-**1**.

Likewise, an experiment with **3** was conducted. After **3** was added to the solution of **11**(CD_3OH), the hydride signal of **19$_{Si}$** (R = H) appeared at δ −19.1 (400 MHz ^1H NMR). The −7% nOe was observed between the signals at δ −19.1 and δ 0.77 (br s). The signal at δ 0.77 is assignable to the olefinic proton(s) of the coordinated **3**, since this signal disappeared under the conditions using **3**-*3*,*3*-d_2 and CD_3OD.

Preparation of RuH(RCOO)[(*S*)-binap]P(C_6H_5)$_3$ (17: R = CH_3, 18: R = *t*-C_4H_9). Ru(CH_3COO)$_2$[(*S*)-binap] [(*S*)-**10**] (347 mg, 0.413 mmol) and P(C_6H_5)$_3$ (113 mg, 0.431 mmol) were placed in a dry 250 mL Schlenk tube, and CH_3OH (60 mL) was introduced under an Ar stream. The solution was degassed by one freeze−thaw cycle and exposed to 1.2 atm of H_2 at 25 °C for 4 h and at 4 °C for 24 h, during which time a yellow solid was precipitated. After releasing the H_2 gas, the supernatant was removed by a cannula covered with a filter paper at one end. The solid was washed with CH_3OH (20 mL) and dried in

vacuo. The yellow-colored solid was dissolved in toluene (10 mL), and hexane (50 mL) was carefully placed on the toluene solution. The resulting two-layer system was kept at 3 °C for 7 days. Removal of the mother liquor was followed by washing with hexane (20 mL) and drying in vacuo, affording yellow powdery crystals of **17** (300 mg, 70% yield): ^{1}H NMR (400 MHz, toluene-d_8) δ −17.8 (1H, ddd, $J_{H,P}$ = 29.0, 25.3, and 23.5 Hz, RuH), 1.18 (3H, s, CH_3COO); $^{31}P\{^1H\}$ NMR (162 MHz, toluene-d_8) δ 40.51 (1P, dd, $J_{P,P}$ = 299.3 and 23.7 Hz), 49.01 (1P, dd, $J_{P,P}$ = 299.3 and 38.5 Hz), 82.78 (1P, dd, $J_{P,P}$ = 38.5 and 23.7 Hz). Anal. Calcd for $C_{64}H_{51}O_2P_3Ru$: C, 73.48; H, 4.91. Found: C, 73.71; H, 4.74.

In a similar way, RuH(*t*-C_4H_9COO)[(*S*)-binap]P(C_6H_5)$_3$ (**18**) was prepared in 72% overall yield from Ru(*t*-C_4H_9COO)$_2$[(*S*)-binap] (101 mg, 0.110 mmol).[64] Conditions: [Ru(*t*-C_4H_9COO)$_2$[(*S*)-binap]] = 9.2 mM, [P(C_6H_5)$_3$] = 10 mM, 1 atm of H_2, CH_3OH, 24 °C, 7 days. The yellow solid (85 mg) was dissolved in the least amount of degassed toluene (1.5 mL) with the aid of heating. Degassed pentane (3 mL) was very carefully added to the solution to form two layers. This was kept at 4 °C for 12 h, affording orange prismatic crystals. This was subjected to an X-ray diffraction experiment (vide infra). mp 168.3−169.5 °C dec ^{1}H NMR (400 MHz, toluene-d_8) δ −18.5 (1H, ddd, $J_{H,P}$ = 29.3, 26.4, and 22.9 Hz, RuH), 0.67 (9H, s, C_4H_9COO); $^{31}P\{^1H\}$ NMR (162 MHz, toluene-d_8) δ 38.4 (1P, dd, $J_{P,P}$ = 299.3 and 20.7 Hz), 48.4 (1P, dd, $J_{P,P}$ = 299.3 and 38.5 Hz), 80.8 (1P, dd, $J_{P,P}$ = 38.5 and 20.7 Hz). Anal. Calcd for $C_{74}H_{65}O_2P_3Ru$: C, 75.30; H, 5.55. Found: C, 75.11; H, 5.45.

X-ray Crystallographic Analyses. The coordinates for all compounds according to X-ray crystallography were deposited with the Cambridge Crystallographic Data Center. The coordinates can be obtained, on request, from the Director, Cambridge Crystallographic Data Center, 12 Union Rd., Cambridge, CB2 1EZ, U.K. Crystals suitable for structure determination by X-ray diffraction were obtained, selected, and mounted as described below.

(a) Ru(CH_3COO)$_2$(CD_3OH)[(*S*)-binap]. Orange platelet crystals were grown from a CD_3OH (0.6 mL) solution of Ru(CH_3COO)$_2$-[(*S*)-binap] (7.8 mg, 9.23 μmol) in a Young's type Schlenk tube of a 5 mm × 15 cm size under 1 atm of H_2 atmosphere and at room temperature. A single crystal with the dimensions of 0.25 mm × 0.20 mm × 0.08 mm was selected by means of a Hampton Research Cryo Loop and immediately mounted on the magnetic base of a goniometer head in a −130 °C nitrogen atmosphere. The crystal encased in the solvent by a flash cooling method was subjected to data collection.

(b) RuH(*t*-C_4H_9COO)[(*S*)-binap]P(C_6H_5)$_3$. The 1:1 cocrystal of RuH(*t*-C_4H_9COO)[(*S*)-binap]P(C_6H_5)$_3$ and toluene was obtained by the procedure described above. An orange prismatic crystal (0.36 mm × 0.30 mm × 0.12 mm) was mounted on the top of a quartz fiber with a small amount of epoxy resin adhesive and transferred to a goniometer head. The data were collected at −130 °C.

(c) Methyl (*Z*)-α-(Acetamido)cinnamate. Colorless platelet crystals were obtained by recrystallization of (*Z*)-**1** (200 mg) using a liquid−liquid diffusion of hexane (6 mL) to ethanol (3 mL) at room temperature. In a similar way to that described in (b), a suitable crystal 1.33 mm × 0.41 mm × 0.11 mm was subjected to data collection at −130 °C.

Acknowledgment. This work was aided by Grants-in-Aid for Scientific Research (Nos. 07CE2004, 05234101, 06226234, 08240101, 00000548, 60000491, and 9900481) from the Ministry of Education, Culture, Sports, Science and Technology, Japan. The authors would like to thank Professor H. Kudo at Tohoku University and Dr. M. Kato at the Atomic Energy Research Institute for making the H_2/HD/D_2 gas analysis system, and Mr. T. Noda for making Schlenks with Young's taps.

Supporting Information Available: Description of preparation of the enamide substrates, kinetic apparatus, kinetic plots over the entire course of the reaction, GC chromatography of gas phase, $^{13}C\{^1H,^2H\}$-^{1}H correlation NMR spectrum, synthesis of authentic isotopomers, and X-ray crystallographic analyses. ORTEP drawings, tables of atomic parameters, anisotropic temperature factors of (*S*)-**10**(CD_3OH), **18**, and (*Z*)-**1** (PDF). This material is available free of charge via the Internet at http://pubs.acs.org.

JA010982N